A Szilikátipari Tudományos Egyesület lapja

építőanyag

Journal of Silicate Based and Composite Materials

A TARTALOMBÓL:

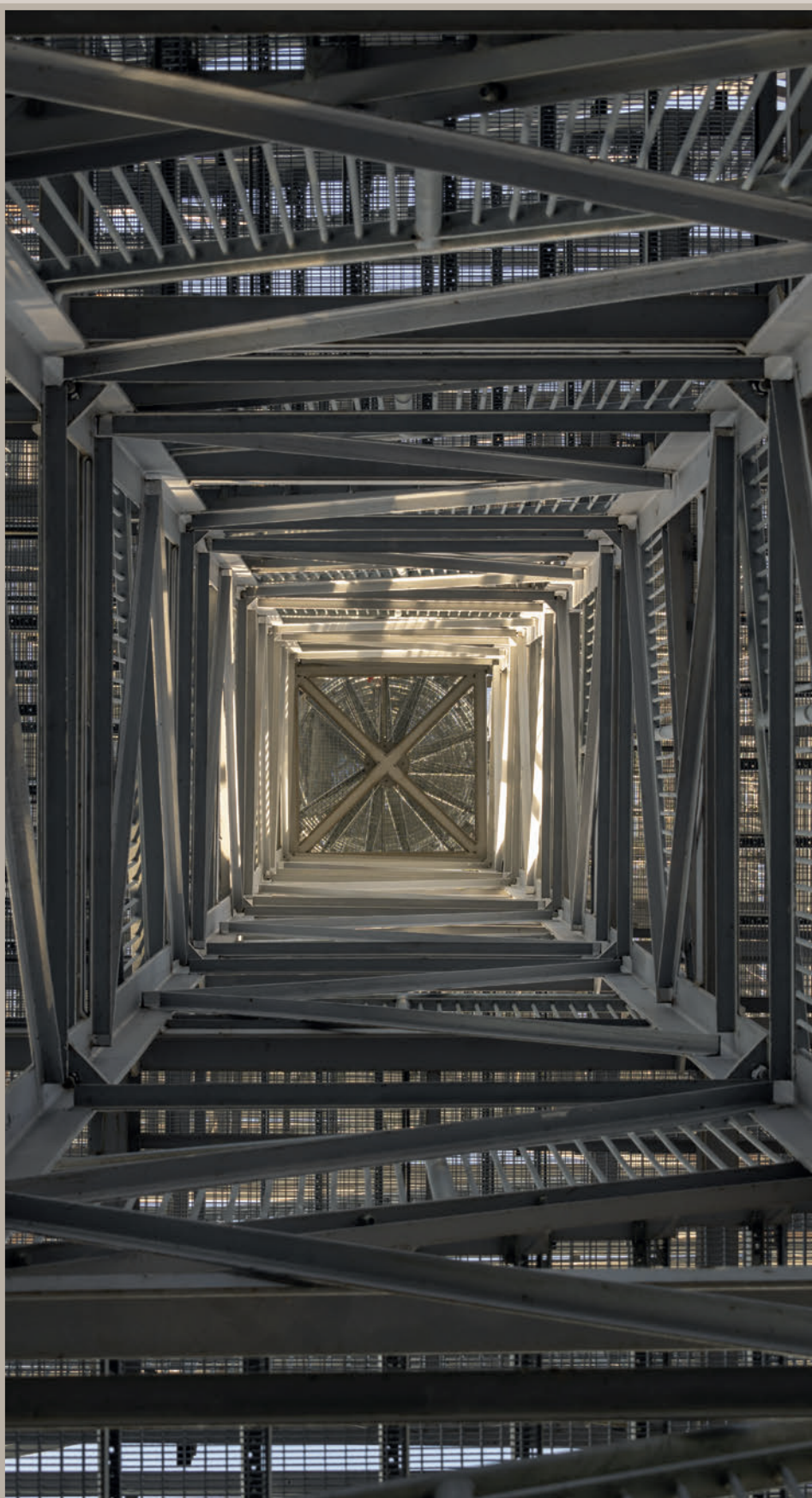

2024/3

The XIXth Conference of the European Ceramic Society will take place from August 31 to September 4, 2025 at the International Congress Center in Dresden, Germany.

On behalf of the European Ceramic Society ECerS, the Deutsche Keramische Gesellschaft DKG, and Fraunhofer Institute of Ceramic Technologies and Systems IKTS, it is our great pleasure to welcome you to the beautiful City of Dresden.

Planned every two years, the ECerS Conference focuses on cutting-edge research and product developments in a wide range of ceramic-related areas. The program provides an opportunity for scientists, researchers, engineers, and industry leaders from around the world to present and exchange their latest findings in ceramic science and technology.

The XIXth ECerS Conference is divided into 14 symposia covering all relevant aspects of ceramic science and technology. It specifically addresses the most important challenges of our society, such as sustainability, energy transition and closed cycle technologies. Moreover, the 100th annual meeting of DKG is fully integrated.

Dresden's beauty is undisputed – and unmistakable it reveals itself to visitors at first glance and is characterised by an irresistible combination of romantic landscape, baroque architecture and one of the most beautiful historic city centres in Germany. At second glance, "Florence on the Elbe", as it is often called, attracts visitors with a wealth of art and culture that can easily hold its own on an international level. The locals love and enjoy their city, its streets and squares and its concert halls with regular performances by world-class artists – and guests from all over the world are very much invited to join in.

Moreover, Dresden is The City of Science in Germany. With 10 Fraunhofer institutes, 4 Max Planck institutes, 5 Leibnitz institutes, 2 Helmholtz institutes and Dresden University of Technology as one of Germanys top ranked Universities of Excellence Dresden has the densest agglomeration of research institutions all over Europe. Dresden also ranks No. 1 in Europe with around 1,500 companies and 48,000 employees in the areas of information and communication technology and microelectronics. Therefore, the conference also serves a hub to discover new R&D opportunities in Europe.

We are looking forward to seeing you in Dresden.

www.ecers2025.org

építőanyag
Journal of Silicate Based and Composite Materials
2024/3

TARTALOM

CONTENT

A finomkerámia-, üveg-, cement-, mész-, beton-, tégla- és cserép-, kő- és kavics-, tűzállóanyag-, szigetelőanyag-iparágak szakmai lapja
Scientific journal of ceramics, glass, cement, concrete, clay products, stone and gravel, insulating and fireproof materials and composites

A folyóiratot referálja · The journal is referred by:
ProQuest · Google Scholar · INDEX COPERNICUS INTERNATIONAL · THOMSON REUTERS

A folyóiratban lektorált cikkek jelennek meg.
All published papers are peer-reviewed.
Kiadó · Publisher: Szilikátipari Tudományos Egyesület (SZTE)
Elnök · President: ASZTALOS István
1034 Budapest, Bécsi út 120.
Tel.: +36-1/201-9360 ▪ E-mail: epitoanyag@szte.org.hu
Tördelő szerkesztő · Layout editor: NÉMETH Hajnalka
Címlapfotó · Cover photo: SIMON Andrea

WWW.EPITOANYAG.ORG.HU
EN.EPITOANYAG.ORG.HU

Online ISSN: 2064-4477
Print ISSN: 0013-970x
INDEX: 2 52 50 ▪ 76 (2024) 93-124

Vol. 76, No. 3

Assessment of basalt micro-fiber for use in cementitious mortar

Maged E. EL-FAKHARANY
Researcher in field of geology, and XRD lab member at Raw Building Materials Technology and Processing Research Institute, Housing and Building National Research Center (HBRC), Cairo, Egypt

M. Ezzat TAHA
Associate Professor in field of geology at Raw Building Materials Technology and Processing Research Institute, Housing and Building National Research Center (HBRC), Cairo, Egypt

Maged E. El-FAKHARANY ▪ Housing and Building National Research Center (HBNRC), Egypt
M. Ezzat TAHA ▪ Housing and Building National Research Center (HBNRC), Egypt
Érkezett: 2024. 02. 20. ▪ Received: 20. 02. 2024. ▪ https://doi.org/10.14382/epitoanyag-jsbcm.2024.10

Abstract
Stiff and durable cement mortar is considered the most widely wanted building materials. The durable cement mortar will decrease the costs of concrete maintain and future repair in the construction work. Basalt fiber (BF) is modified to different specific micro sizes to basalt micro-fiber (BMF) in order to achieve good mechanical with better microstructural properties of the casted cementitious mortar. This paper verifies the improvements that are made to the cement by the prepared basalt micro fibers BMF1 and BMF2 with different replacement contents (0.2, 0.5 and 1%) of the cement. All BMF additions influence on the physico-mechanical properties of the casted cementitious mortar. Low BMF replacement ratios led to an significant increase in the mechanical properties whereas, the higher replacement 1% shows slightly decreasing than the control sample. The modified BMF1 with replacement 0.2% show the highest value in both compressive and split tensile strength, it also show compacted microstructure by increase cohesion forces between particles in the mix. The more finely modified BMF2 show tiny micro equant particles beside the retained small fiber shape due to the relatively longer time of specific grind leading to dense mortar and helping in inhibit connected pores in the mortar internal microstructure. Finally, It has become important to discuss the modify BF and recommended to use the BMF in case of enhancement cementitious mechanical strength.
Keywords: Basalt Micro-fiber; Cementitious Mortar; Mechanical Properties; Internal Micro-structure.
Kulcsszavak: bazalt mikroszál, cementhabarcs, mechanikai tulajdonságok, belső mikrostruktúra

1. Introduction

Basalt is a widely distributed type of volcanics formed by the rapid cooling of lava at the surface of the earth. So, it is the most common rock in the Earth's crust. Fibers can be formed from molten basalt stone at high-temperature by extrusion. The basalt can be melt (1300-1700 °C) and spin into hairy fine fibres, where high quality fibers are made from basalt deposits with uniform chemical makeup [1]. The resulting basalt fibers chemically are containing 45%–52% SiO_2, and are considered environmentally friendly and non-hazardous materials. Basalt fibers have excellent properties such as high-modulus, high-heat resistance, sound insulation and thermal stability [2]. Also their processing and physical property leads to decreases in production costs which make it less expensive than alternative glassy fibers [3-4]. Basalt fibers are also show good abrasion resistance and less prone to damage from aggressive salts, alkali or acid solutions [5–9]. These excellent properties facilitate many potential applications especially in building material industry. Researchers have used basalt fibers as a reinforcing material in concrete manufacturing due to its good mechanical characterization. It used for reinforcing concrete alone or modified with other additives [10–17]. As well as, it can be chopped and grinded as cement additive to gain high mechanical properties [18-20].

Fibers have been added to concrete and mortar for many years in order to reduce the amount and size of cracks. It show better binding properties of cementitious composite due to the similarity of chemical properties [21]. In addition to the physical parameters as fiber length, fiber concentration and temperature condition can effect on mechanical properties and enhance the concrete strength [22]. There is an advice to study the effect of basalt fiber with different modification [23]. It can be modified by many methods leading to improve the internal structure of cementitious matrix. So, the effect of the modified basalt fiber size may make significant change in mechanical properties of the cement mortar when it modified to different micro lengths. The main aim of this research is to clarify the effect of the modification of the basalt fiber to the size of micro-fiber (BMF) and significant changes in mechanical and micro-structural properties of the cement mortar modified with different percentages and micro sizes, showing the optimal micro length and its cement replacement level with BMF.

2. Materials and methods

2.1 Materials

The materials used in the research (cement, sand, basalt fiber) are analyzed by XRF and XRD, and are found identical to the Egyptian standard specifications [24]. Their major oxides are listed in *Table 1*. The used cement is Egyptian Ordinary Portland Cement (CEM II with Rank 42.5) produced by Beni-Suef Cement Company. The sand is composed mainly of quartz mineral and it is sourced from a common quarry around Cairo district, Egypt, serves as fine aggregate in the mix design. Basalt fibers were supplied by a company called Rockal specialized in the manufacturing of Rock fibers. Basalt fibers are shown to be amorphous when examined by XRD and having silica content 41% estimated by XRF as shown in *Table 1*.

Material	Major oxides by XRF													
	SiO_2	Al_2O_3	Fe_2O_3	CaO	MgO	TiO_2	Na_2O	K_2O	P_2O_5	SO_3	MnO	LOI	Total	Mineral content (XRD)
Basalt fiber	41.01	12.10	11.0	23.90	5.20	2.69	2.04	1.19	0.27	0.20	0.19	0.03	99.91	amorphous
Sand	97.30	0.08	0.24	1.50	0.11	0.01	0.19	0.41	0.00	0.04	0.00	1.33	99.81	Quartz
Cement (OPC)	20.05	4.69	3.52	62.00	1.61	0.40	0.40	0.19	0.16	2.39	0.09	4.40	99.90	

Cement specific gravity = 3.11 , Ins.Res = 1.27

Table 1 Chemical composition of the used materials by XRF
1. táblázat Használt anyagok kémiai összetétele XRF alapján

2.2 Preparation of BMF

The basalt fiber as received average length is about 10 cm with individual fiber diameter approximately 10 μm. The sequence of preparation of the BMF is as follow; firstly, basalt fibers are separated with hand into individual fibers to use as it is and in order to be uniformly distributed in the mix. Secondly, a small fraction from the basalt fibers bundle is fed to the grinding machine by feed capacity (50 g/L) and grinded on two intervals, 30 sec and 300 sec. and termed BMF1 and BMF2 corresponding to 30 sec and 300 sec respectively.

2.3 Mixing procedure

Mortar Mix	Mix proportions (kg/m³)				
	Cement	Sand	BMF	water	Super Plastizer
Control	568	1670	0	212.8	2.8
BMF0-0.25%	558.6	1670	1.4	212.8	2.8
BMF0-0.5%	557.2	1670	2.8	212.8	2.8
BMF0-1%	554.4	1670	5.6	212.8	2.8
BMF1-0.25%	558.6	1670	1.4	212.8	2.8
BMF1-0.5%	557.2	1670	2.8	212.8	2.8
BMF1-1%	554.4	1670	5.6	212.8	2.8
BMF2-0.25%	558.6	1670	1.4	212.8	2.8
BMF2-0.5%	557.2	1670	2.8	212.8	2.8
BMF2-1%	554.4	1670	5.6	212.8	2.8

Table 2 Mix proportion of the studied cementitious mortars
2. táblázat A vizsgált cementkötésű habarcsok keverési aránya

In order to evaluate the effect of BMF blended with cement on the physical and mechanical properties of BMF cement based mortar, OPC is mixed with sieved sand passing 1.18 mm sieve in ratio equals 1/3 to form a control sample with 0% BMF and utilizing water-to-cement ratio (w/c) 0.38. Secondly, mixing BMF with cement by weight replacement (0.25, 0.5, and 1%) standing for BMF0, BMF1 and BMF2 as shown in *Table 2*. Then dry density and water absorption are measured for each mix according to [25], also, compressive and split tension strength evaluated for each mortar mix following the Egyptian standard code [24]

3. Results and discussions

3.1 Size characteristics

3.1.1 Particles distribution of modified BMF

The effect of size modification of BMF on the cementitious mortar, particle size estimation for BMF samples (BMF1 and BMF2) is performed by laser particle size. The results showed the particle size distribution of the BMF1 sample ranged from 451μm to 0.6 μm length with a mean size (112 μm), as shown in *Fig 1*. However, the BMF2 sample that was subjected to relatively longer time of grinding (300 sec), it is obvious that it became more finer showing fibers dimension ranged between 251 μm:0.5 μm with a mean size equal 6 μm (*Fig 2*).

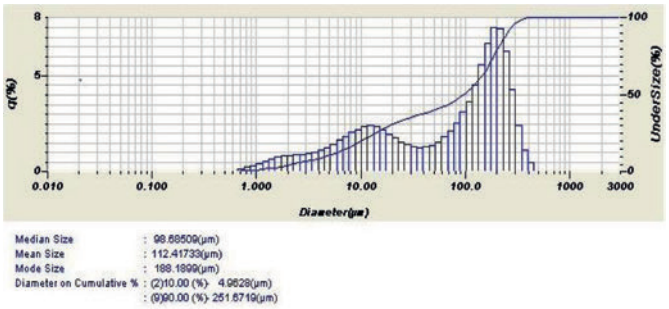

Fig. 1 Laser scattering Particles size distribution chart of BMF1 (30 sec)
1. ábra BMF1 (30 mp) szemcseméret-eloszlási diagramja lézerszórással

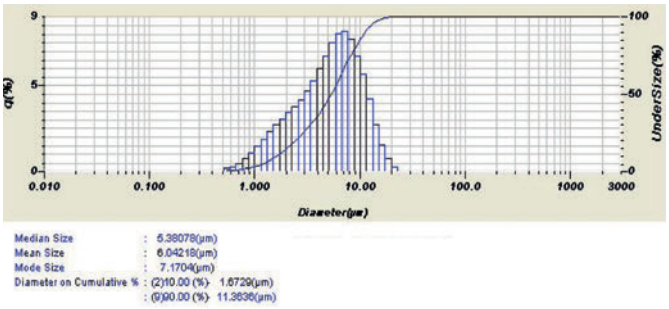

Fig. 2 Laser scattering Particles size distribution chart of BMF2 (300 sec)
2. ábra BMF2 (300 mp) szemcseméret-eloszlási diagramja lézerszórással

3.1.2 Microscope examination

Examination of size modified BMF0 sample using optical microscope (*Fig. 3.a*), which is chopped by hand show long fiber structure. Also, the examination of BMF1 sample revealed that most of its particles show large to medium micro fibers length and retained its fiber shape after suffered to 30 sec

of grinding. However, the BMF2 sample with longer time of grinding show lesser and smaller micro fibers beside to scattered small angular micro particles (*Fig. 3.c*) indicating the beginning of losing fibrous structure.

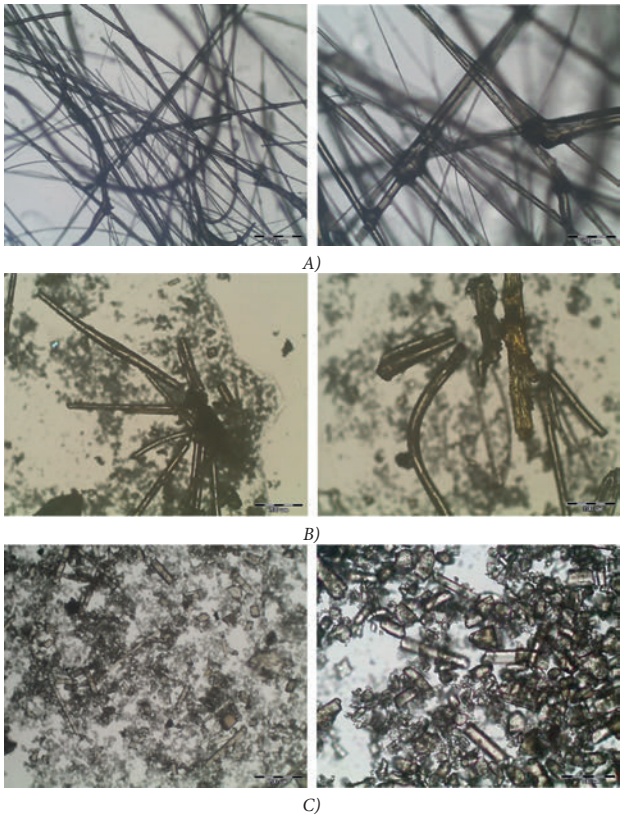

Fig. 3 Photomicrographs of BMF A) fibers network of BMF0 sample with magnification (left -4X) and (right-10X), B) micro fibers of the sample BMF1 (10X magnification) at left and (20X magnification) at right, C) Distribution of equant micro particles beside to microfibers of BMF2 sample with magnification (10X) to the left and (20X) to the right

3. ábre BMF mikrofotók A) BMF0 minta szálhálózata nagyítással (balra -4X) és (jobbra -10X), B) BMF1 minta mikroszálai (balra 10X nagyítás) és (jobbra 20X nagyítás), C) BMF2 minta egyenletes mikrorészecskéinek eloszlása a mikroszálak mellett, nagyítással (balra 10X) és (jobbra 20X)

3.2 Dry density

There is hardly noticeable difference in dry density between all the studied mortars prepared by the modified BMF at low cement replacement levels (0.25, 0.50, and 1.00%). However the density values decreased from 2.392 kg/cm^3 of the control sample (0% replacement of BMF) to 2.376 kg/cm^3 at the highest replacement level of the sample (BMF0-1%). And the modified BMF1 sample show slight decrease in the density from 2.388 of (BMF1-0.25%) to 2.382 kg/cm^3 with the highest replacement (BMF1-1%). While the modified BMF2 samples show slightly relative increase in density values compared to BMF0 and BMF1 samples as shown in *Fig. 4*. That may relate to the differences in fiber size and shape of the three modified types. From the concept of cementitous mortar density may affect its strength as discussed by authors [26]. These relatively increasing density values of BMF2 are considered reasonable to a good mortar if compared with other mixes, as it can lead to more compaction by finer fibers interaction with other particles in the mix.

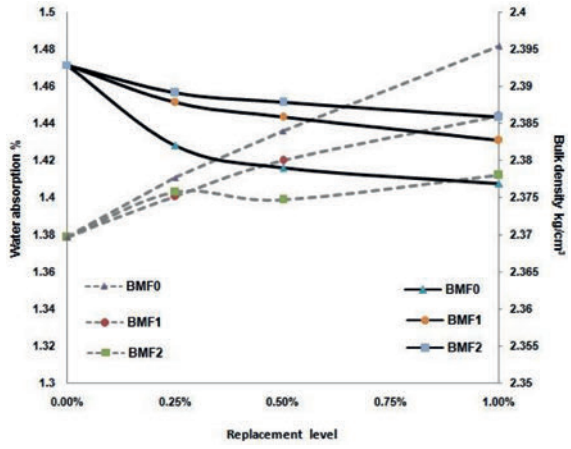

Fig. 4 A relation showing mortar dry density versus water absorption using prepared BMF of different sizes

4. ábra A habarcs száraz sűrűsége és vízfelvétele közötti összefüggés különböző méretű előkészített BMF-ek használatával

3.3 Water absorption

The water absorption property is very important for special mortar types, since it is used for determined the quality of the mortar and its application [23]. There is direct relation between the water absorption values and bulk density of mortars mixed by BMF as shown in (*Fig. 4*). The fact that low density due to increase in voids content between particles leads to higher water absorption, may be explained that replacement by 1% of BMF0 and BMF1 show the highest water contents between all samples equals 1.48 and 1.44% respectively, than mortar with finest fibers (BMF2) which equals 1.41%. That is explained further by increasing of voids since grain size distribution of studied BMF may stifle filling cavities especially in the case of hand chopped basalt fiber (BMF0) also the relatively higher in modified fibers length as in case of (BMF1).

3.4 Compressive strength

Compressive strength was evaluated by testing moulded mortar cubes according to the Egyptian code for each BMF mix. There is a variation in strength values by using different modified BMF with different cement replacement levels (0.2, 0.5, and 1%). The control sample reached compressive strength value 30.5 MPa and evaluated as class (C30). The compressive strength after 28 days increased about 5.0, 20.6 and 6.9% when using in the mix 0.25% of BMF0, BMF1 and BMF2 respectively. However, the replacement value 0.5% show slightly decreasing in value reached to 29.6, 32.6, 32.1 MPa when cement replaced by (BMF0, BMF1 and BMF2) respectively. In addition to the cement replacement with 1% of (BMF0, and BMF1) decrease the strength with 9.5 and 0.2% of the control sample respectively. Unlike 1% of (BMF2) show very slightly increase in the compressive strength. That means the optimum replacement value of the BMF mortar may be (0.5%) or (1%) depending on the method and time of mechanical modification. However cement replacement level (0.25%) shows the highest values especially in the mortar mix with BMF1 may relate to the good physical properties of this cementitious mortar [25]. On the other hand, the finer BMF2 obtained by 300 second of grinding seems to be more effective for keep strength than others. This may explained as the smaller

fiber length may easily distribute in the mixture resulting in higher bond strength between the micro fiber filaments and the other mix particles. That helps more specific surface of fibers to interact with the cement making good compaction. Their terminals give a connecting growing pattern providing the materials a higher strength [19]. Therefore using modified BMF in cementitious mortar mix may help in strengthening objects.

3.5 The split tensile strength

The split tensile strength of BMF mortars show to some extent similarity to compressive strength curves (*Fig. 5*). Tensile strength values increased with all the replacement percents (0.25, 0.5 and 1%) by the prepared basalt microfiber (BMF0, BMF1 and BMF2). that is attributed to the fibers bridging interaction [23], where the mortar ductility is improved preventing further crack growth [27-28]. All tensile strength values varies between 2.25 and 3.87 MPa which is considered higher than the control value (2.04 MPa) up to 1% replacement, unlike the compressive strength values with 1% replacement by (BMF0, BMF1). It mentioned that BMF had no effect on the compressive strength but might significantly improve the tensile strengths [9].

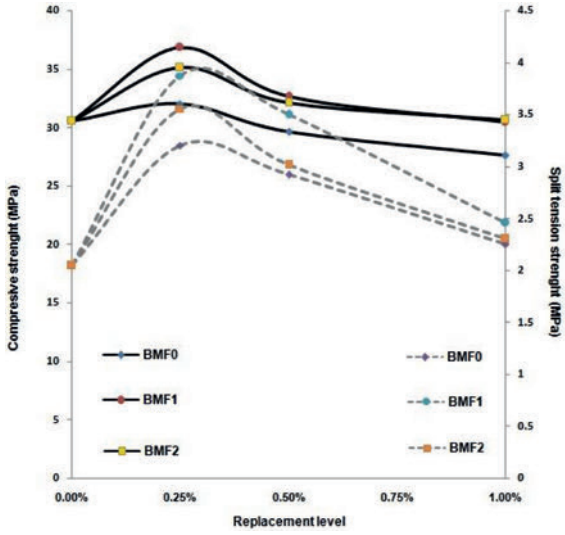

Fig. 5 A graphic relation between compressive strength and split tension strength of BMF mortars
5. ábra A BMF habarcsok nyomószilárdsága és hasító húzószilárdsága közötti grafikus összefüggés

However there is a decreasing with increasing replacement percent up to 1%. Also there are a noticeable difference between the three prepared BMF used. The mortar samples mixed with BMF0 without grinding show the lowest split tensile strength values (3.20, 2.92 and 2.25 MPa) with the alternatives (BMF1 and BMF2). This may attributed as discussed by [9] to the increasing fiber content which give negative effect on workability which reflect segregation and poor fiber distribution may occur. Thus the perfect mechanical adherence with high BMF content may be prevented from occurring especially with continuous longer fiber filaments in case of BMF0 using as it is. The samples with finer micro fibers (BMF2) which showed good compaction unexpectedly showed relatively decrease in split tension strength values (3.55, 3.01 and 2.30 MPa) than values of (BMF1) samples (3.87, 3.50 and 2.46 MPa) with (0.25, 0.5 and 1%) replacement respectively. That may attributed to more grinding time (5 m) begin to destroyed the fiber structure but in case of BMF1 the fiber shape is still retained with more sharp terminals which may make a good kind of internal tension with hydrated cement particles.

3.6 Scanning electron microscope of BMF mortar

The morphological structure of different BMF mortar mixes were visualized using SEM (*Fig. 6*). Control mortar sample described by dense homogeneous cement paste however there are few micro cracks and micro voids accompanied the periphery of sand aggregates. Most of mortar samples with BMF illustrate that fibers act as a bridge between cement paste grains, that simply explain the better strength gained by using basalt microfibers. However, increasing content of BMF by relatively higher replacement 1% may accompany by fiber agglomeration lead to poor distribution of the fiber in the mix.

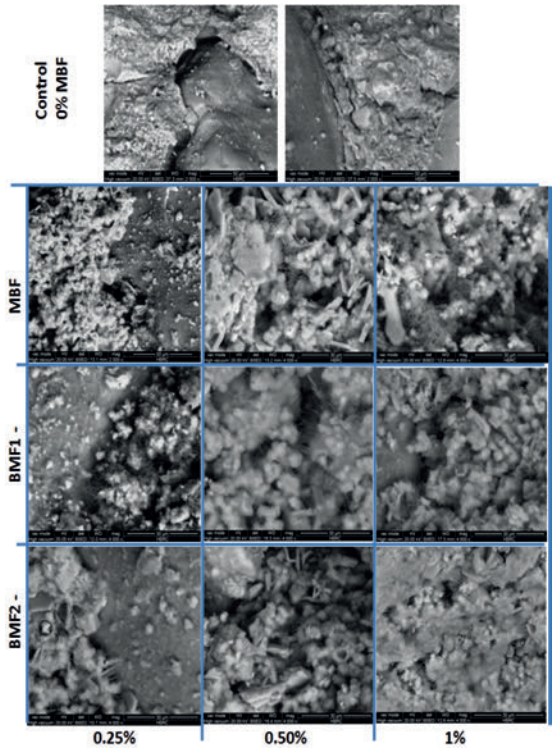

Fig. 6 SEM micrographs of the different studied BMF mortar mixes
6. ábra SEM felvételek különböző vizsgált BMF habarcsokról

Mortar samples with BMF1 show better fiber distribution, more compaction and void filling improvement than the unmodified BMF due to the increase of its role as abridge linkage filling voids. Finer particles and specific short fibers length of such samples may help for well distribution within the cement matrix. Micrographs of BMF2 mortar samples illustrate to some extent similarity to BMF1 samples, however there is an appearance of more compaction if compared with other mixes. The dense appearance of that samples may explained by finer microfibers and tiny equant shape micro particles formed by longer grind help in good distribution and well fishering with other particles in the mortar mix. It is noticed that BMF2 may lead to decrease the possibility of formed micro pores within the cement matrix or around the aggregates periphery.

4. Conclusion

Micro basalt fibers can be used as admixtures for cementitious mortar. Basalt micro fiber can be prepared by grinding for different specific time (30 or 300 sec) to yield micro fibers with a mean size about (112 μm) and (6 μm). Grinding effect can change the fiber shape where basalt fiber grinded for longer time can lose its fiber structure.

It is preferable to use BMF with prepared micro fiber sizes than unmodified fiber. Preparation and modification of BMF will help in well distribution in the mortar during mixing. Basalt fiber characteristics in micro length have a slightly influence on the physical mortar properties especially its density and w absorption ability. Increasing of BMF content prepared with different micro fiber lengths can increase the water ability of the cementitious mortar and lower its density. Types of fibers and their characteristics sizes can control the differences of the studied mortar water absorption.

Modified BMF can enhance the mechanical properties of cementitious mortar since it increases both its compressive and tension strength. Especially split tension strength results showed more positive effect with BMF than the compressive strength of the same mortar samples. And that in very fine micro sizes basalt fibers that retained the hairy fiber shape can perform well than others fibers which loses its fiber shape. Because of the fiber filaments still have sharp terminals which make a good kind of internal tension with hydrated cement particles. Therefore, using prepared BMF in cementitious mortar mix can help in concrete strengthening purposes.

Finally, the prepared BMF with the specific micro sizes effectively will be positive the internal microstructure of the cementitious mortar giving more dense and compacted appearance due to the modified basalt fiber particles concluded that using BMF will be a good step for improving mortar characteristics.

References

[1] Ansari. P., Chandak. R., Strength of Concrete Containing Basalt Fibre. Int. Journal of Engineering Research and Applications, Vol. 5, (2015), pp.13-17

[2] Novitskii. A., High-temperature heat-insulating materials based on fibers from basalt-type rock materials, Refract. Ind. Ceram. Vol.45(2) , (2004), pp.144-146.

[3] Sim. J., Park. C., and Moon. D., "Characteristics of basalt fiber as a strengthening material for concrete structures," Compos. Part B-Eng.Vol. 36, (2005), pp.504- 512.

[4] Artemenko, S. E., and Kadykova, Y. A. "Polymer composite materials based on carbon, basalt, and glass fibres," Fibre Chem. Vol. 40(1), (2008), pp30-32

[5] Singha. K., A short review on basalt fiber, International Journal of Textile Science Vol.1 (4), (2012), pp.19-28.

[6] Kabay. N., Abrasion resistance and fracture energy of concretes with basalt fiber, Construction and Building Material Vol.50, (2014), pp. 95–101. https://doi.org/10.1016/j.conbuildmat. 2013.09.040

[7] Elshafie. S., Whittleston. G., A Review of the Effect of Basalt Fiber Lengths and Proportions on the Mechanical Properties of Concrete, International Journal of Research in Engineering and Technology, Vol. 4, 2015, pp. 458-465. https://doi.org/10.15623/ijret.2015.0401069

[8] Yakov. L., Sergey. G., & Mikhail. M., Zhukovskaya. E., Lazoryak. B., High alkali-resistant basalt.fiber for reinforcing concrete. Materials & Design, (2015), 73. https://doi.org/10.1016/j.matdes.2015.02.022

[9] Guo. Z., Wan. C., Xu. M., and Chen. J., Review of Basalt Fiber-Reinforced Concrete in China: Alkali Resistance of Fibers and Static Mechanical Properties of Composites, Advances in Materials Science and Engineering, (2018), Vol. 2018, p12.

[10] Ding. Z., Lu. Z., Li. Y., Feasibility of Basalt Fiber Reinforced Inorganic Adhesive for Concrete Strengtening, Advanced Materials Research Vol. 287-290 (2011) pp 1197-1200

[11] Wei. B., Song. S., Cao. H., Strengthening of basalt fibers with nano-SiO_2–epoxy composite coating, Materials and Design, Vol.32, (2011), pp.4180-4186

[12] Borhan. T., Properties of glass concrete reinforced with short basalt fibre, Materials and Design, Vol.42, (2012), pp.265–271

[13] Huang. D., Xiong. Q., and Xing. Z., Effect of Dipping Basalt Fiber on Mechanical Properties of Concrete, 2015, 3rd International Conference on Material, Mechanical and Manufacturing Engineering (IC3ME 2015), pp.2026-2030

[14] Ayub. T., Shafiq. N., Nuruddin. M. F., Mechanical properties of high-performance concrete reinforced with basalt fibers. Proced Eng, Fourth (2014), 77:131–139

[15] Girgin. Z., Yıldırım. M., Usability of basalt fibres in fibre reinforced cement composites, Materials and Structures, Vol49, (2016), pp 3309–3319

[16] Rashad. A. M., A synopsis about the effect of basalt and natural fibers on geopolymer properties, Natural Resources Conservation and Research, Volume 1, (2018), 9P. https://doi.org/10.24294/nrcr.v1i2.752

[17] Al-Kharabsheh. B., Arbili. M., Majdi. A., Alogla. S., Hakamy. A., Ahmad. J., Deifalla. A., Basalt Fiber Reinforced Concrete: A Compressive Review on Durability Aspects. Materials, 16, 429, (2023), pp1-22

[18] Katkhuda. H., Shatarat. N., Improving the mechanical properties of recycled concrete aggregate using chopped basalt fibers and acid treatment. Construction and Building Materials, 140, (2017), pp 328–335

[19] Bazhcnov. V., Chervontseva. M., Application of Modified Basalt Microfiber in Concrete, 2018, MITU-MASI Bulletin No.3, (2018), pp.21-26

[20] Ralegaonkar. R., Gavali. H., Aswath. P., Abolmaali. S., Application of chopped basalt fibers in reinforced mortar: A review, Construction and Building Materials, Vol.164, (2018), pp 589-602.

[21] Yildizel. S., Calis. G., Design and optimization of basalt fiber added lightweight pumice concrete using Taguchi method, Romanian Journal of Materials, 49 (4), (2019), pp.544 -553

[22] Xu. L., Song. D., Liu. N., Tian. W., Study on Mechanical Properties of Basalt Fiber Reinforced Concrete with High Content of Stone Powder at High Temperatures, 2021, Advances in Materials Science and Engineering, Vol 2021, 15p.

[23] Liu. H., Yu. Y., Liu. Y., Zhang. M., Li. L., Ma. L., Sun. Y., Wang. W., A Review on Basalt Fiber Composites and Their Applications in Clean Energy Sector and Power Grids. Polymers, Vol.14, 2022, 20p. https://doi.org/10.3390/polym14122376

[24] ECP-203. (2023): Egyptian Code for the design and implementation of concrete structures, Manual of testes, copy2023, HBNRC, Giza, Egypt, 132p

[25] ASTM C642. (2013): Standard test method for Density, Absorption and Voids in Hardened Concrete, ASTM International, West Conshohocken, PA, www.astm.org

[26] El-Fakharany, M. E. – Ezzat, M. – Gad, A. – Ghafour, N. G. Abdel – Baghdady, A. R.: Performance of dolomitic cementitious mortars as a repairing material for normal concrete in Egypt Építő anyag – Journal of Silicate Based and Composite Materials, Vol. 71, No. 2 (2019), 33–42. p. https://doi.org/10.14382/epitoanyag-jsbcm.2019.7

[27] Yang. J.J., Guo. J.H., Zhang. L., Guo. L., Comparing and Analyzing Influence of Basalt and Carbon Fibers on the Cement Mortar. Adv. Mater. Res. Vol. 354–355, (2012), pp. 78–82. https://doi.org/10.4028/www.scientific.net/AMR.354-355.78

[28] Zhang. Y., Zheng. Y., Du. C., Hu. S., Wang. Z., Hybrid effects of basalt and polyvinyl alcohol fibers on the mechanical properties and macro-microscopic analysis of low-heat portland cement concrete, Journal of Materials Research and Technology, Vol. 25, (2023), pp 608-632. https://doi.org/10.1016/j.jmrt.2023.05.220

Ref.:
El-Fakharany, Maged E. – **Taha**, M. Ezzat: *Assessment of Basalt Micro-Fiber for Use in Cementitious Mortar*
Építőanyag – Journal of Silicate Based and Composite Materials, Vol. 76, No. 3 (2024), 96–100 p.
https://doi.org/10.14382/epitoanyag-jsbcm.2024.10

Enhancing fire resistance of concrete through metakaolin substitution: A comprehensive experimental study

Zubair YOUSUF
Construction Technology MSc, He is currently pursuing his PhD in Budapest University of Technology and Economics, with research specializing in sustainable construction materials. His work focuses on evaluating the fire resistance and mechanical performance of eco-friendly materials to promote sustainability in construction practices.

Viktor HLAVIČKA
Structural Engineer MSc, PhD, concrete technologist, fire safety engineer, Assistant Professor of Department of Construction Materials and Technologies, Budapest University of Technology and Economics. His main fields of interest are experimental investigation and modelling of fastening systems in concrete and thermally damaged concrete. He is a member of the Hungarian Group of *fib*.

Zubair YOUSUF ▪ Budapest University of Technology and Economics, Department of Construction Materials and Technologies ▪ zubair.yousuf@edu.bme.hu
Dr. Viktor HLAVIČKA ▪ Budapest University of Technology and Economics, Department of Construction Materials and Technologies ▪ hlavicka.viktor@emk.bme.hu

Érkezett: 2024. 06. 21. ▪ Received: 21. 06. 2024. ▪ https://doi.org/10.14382/epitoanyag-jsbcm.2024.11

Abstract
In the pursuit of sustainable construction practices, the use of eco-friendly materials in concrete production has garnered considerable interest. This study meticulously analyzes and compares conventional concrete with concrete incorporating metakaolin as a cement substitute, focusing on its impact on fire resistance properties. It examines mechanisms such as metakaolin's influence on other mechanical properties. A systematic experimental approach assesses the fire performance of concrete specimens with varying metakaolin proportions (5%, 10%, and 20%). These specimens were tested for pre- and post-fire compressive strength, flexural strength, porosity, density, and water absorption. Results indicated that 5% metakaolin provided comparable fire resistance and compressive strength to conventional concrete, although density decreased while porosity increases with higher metakaolin content. The study also addresses the practical implications of using additive-enhanced concrete in real-world construction. This research underscores the importance of environmentally friendly construction solutions while ensuring concrete's durability and safety under fire conditions, contributing to the understanding of sustainable concrete materials and their fire-resistant performance.
Keywords: Metakaolin, Fracture Energy, Elevated temperature, Flexure tensile strength
Kulcsszavak: metakaolin, törési energia, magas hőmérséklet, hajlító-húzószilárdság

1. Introduction

Calibrated kaolinite clay is the source of metakaolin, a pozzolanic substance that is distinguished by its composition of thermally activated alumino silicates. As a primary product as opposed to a secondary or by-product, metakaolin stands out from typical pozzolans. The concrete has a lighter color when metakaolin is present. By accelerating the hydration of ordinary Portland cement (OPC), filling the void, and initiating a pozzolanic reaction with calcium hydroxide ($Ca(OH)_2$), metakaolin strengthens and prolongs the life of concrete [1, 2]. It is acknowledged that the principal factor causing the susceptibility seen at the interface between cementitious materials and aggregate particles is calcium hydroxide ($Ca(OH)_2$). It consequently has a major effect on the properties of concrete that are connected to durability, porosity, permeability, and strength [3, 4]. Concrete loses some of its qualities when it is exposed to high temperatures, like during a fire. This involves serious problems such as decreased compressive strength, spalling and fissures, harm to the link between aggregates and cement paste, and slow degradation of the hardened cement paste. Pozzolanic materials can be used to replace regular Portland cement, improving the cement's mechanical and fire resistance qualities [5]. However, it is possible to lower down the negative effects of temperature on concrete, nevertheless, by taking preventative steps, such as choosing the right materials. The monitoring and prediction of concrete behavior is greatly aided by an understanding of the material properties, including those of cement paste, aggregate, the link between aggregate and cement paste, and the thermal compatibility of their combination [6]. Concrete's ability to withstand fire is largely influenced by the materials that are used. Concrete's ability to withstand fire is discovered to be significantly influenced by the pozzolans that are typically added to it to increase its strength and endurance. To counteract the structural degradation of concrete, researchers have investigated using other binders or adding cement substitutes in part. Materials like silica fume, metakaolin and other supplemental cementitious materials are currently showing promise as feasible solutions that satisfy a range of performance, cost, and environmental requirements [7, 8]. The temperature range that is required to calcine metakaolin usually ranges from 550 °C to 700 °C, which has benefits for sustainability. In comparison to the energy and temperature requirements for clinker manufacturing, which normally calls for temperatures of over 1400 °C, this temperature range is much lower [9]. This suggests that the manufacture of metakaolin requires less energy and money than the production of cement, acknowledging that regular Portland cement is a significant source of carbon dioxide emissions. Furthermore, metakaolin enhances the performance of construction projects by means of its filler effect and pozzolanic chemical reaction with $Ca(OH)_2$. Among other advantages, this improvement includes greater resistance to sulfate, decreased shrinkage and creep, decreased chloride infiltration, and better durability

and service life [10]. This paper conducts a thorough review of existing literature on the impact of metakaolin (MK) on heated concrete properties. It also examines current carbon dioxide (CO_2) emissions in the cement industry and explores how metakaolin could potentially reduce CO_2 emissions and promote environmentally friendly building practices. The substitution of metakaolin (MK) for cement in concrete has been found to enhance mechanical and durability properties, particularly with an optimized replacement ratio. The effectiveness of this ratio is influenced by the characteristics and fineness of the metakaolin. For this study, four concrete mixes containing 0%, 5%, 10%, and 20% metakaolin were prepared and then subjected to high temperatures for analysis.

2. Experimental Study

2.1 Materials

The cementitious material used in all mixtures included ordinary Portland cement Cem I (52.5 N), in compliance with EN 197-1:2011 standards, and metakaolin (Metaver) meeting the NF EN 206-1/CN specifications. To achieve the adequate consistency superplasticizer MasterGlenium 300 was added in varying dosages across the four mixes. *Table 1*, based on the manufacturer's data, provides a comprehensive overview of the chemical composition and the physical and mechanical properties. The fine aggregate used in the mixtures was natural sand, and natural quartz gravel was utilized as the coarse aggregate, both conforming to the standards specified in EN 12620:2002+A1:2008. *Table 2* provides detailed information on particle size, mixing ratios of the aggregates. Standard potable tap water, in accordance with EN 1008:2002, was used for producing and curing the concrete specimens.

2.2 Mix proportions

Four concrete mixes were developed, each with a water/cement (w/c) ratio of 0.45 and 390 kilograms of cementitious material per cubic meter. These included a control mix with 0% metakaolin and three other mixes incorporating metakaolin at 5%, 10%, and 20%, respectively. *Table 3* details the specific proportions of each concrete blend with varying metakaolin content.

Component (%)	Cement (CEM I, 52.5 N)	Metakaolin (MK)
SiO_2	19.73	51.8
Fe_2O_3	3.21	45.8
Al_2O_3	5.55	0.35
CaO	65.02	0.01
MgO	1.44	0.03
SO_3	2.88	-
Na_2O	-	0.13
K_2O	0.78	0.06
Cl	0.0048	-
Specific surface area	4500	22000
Colour	Grey	white

Table 1 Properties of cement (Cem) and Metakaolin (MK)
1. táblázat Cement (Cem) és metakaolin (MK) tulajdonságai

	Fine aggregate Natural Sand	Coarse aggregate Natural Aggregate
Particle size (mm)	0/4	4/8
Mixing ratio (%)	43	57

Table 2 The particle size, Mixing ratio, of aggregates
2. táblázat Adakékanyag szemcseméret, keverési arány

2.3 Mixing, casting, curing, heating, and cooling details

Concrete incorporating Metakaolin (MK) was mixed, poured, and compacted according to EN 12350-5:2019 standards. Mixing was done using a power-driven rotating pan mixer, and samples were cast and compacted using a vibrating table. Fresh concrete was poured into molds and left to set for 24 hours in the lab. After demolding, specimens were submerged in a water tank at 23 ± 1 °C for a week. After one week of water tank curing, they were conditioned in the lab for about 21 days. The test specimens were dried before the heat load to avoid the spalling effect. They were dried at 60 °C for four days. Specimens were then heated in an electric muffle furnace to target temperatures of 20, 100, 200, 300, 400, 500, 600, and 800 °C. Heating started at room temperature, with the temperature rising at a rate of 5 °C to 6 °C per minute until reaching the target temperatures. Specimens were held at these temperatures for 2 hours under steady-state conditions. After heating, the furnace was turned off, and specimens were allowed to cool slowly in ambient air for 24 hours.

2.4 Testing procedure and methods

The Compressive strength (*fc*), Flexure strength (*fl*), Water absorption (*Wa*), Density (ρ), and Porosity (*P*) and Fracture energy (*Gf*) were evaluated for control concrete (0%) and concrete with 5%, 10%, and 20% metakaolin. The fc and fl tests were conducted according to EN 12390-3:2019 Part 3 and EN 12390-5:2019 Part 5 on cubic specimens (15 cm sides) at 14, 28, and 90 days, and on prisms (27 x 7 x 7 cm) at an average age of 40 days. Post-fire compression tests (fcp) were carried out on half prisms (7 cm sides) after exposure to temperatures ranging from 20 to 800 °C at an average age of 46 days. The compressive strength (fc) was measured using a 3000 kN capacity compression machine at a loading rate of 0.6 MPa/s. Flexural tensile strength was determined with a flexural tensile testing machine, adhering to EN 12390-5:2019 Part 5 standards. Water absorption (Wa) tests were performed on 7 x 7 x 7 cm concrete cubes following EN 1936:2007. Twelve specimens per mix were tested at an average age of 40 days. The water absorption was calculated by immersing dried samples (Msd) in water at 20 ± 2 °C until constant mass (Ms) was achieved. The water content (Wc) was derived from the difference between the saturated (Ms) and dried (Msd) masses. The water absorption percentage (Wa) was calculated using the appropriate equation.

$$Wa\ (\%) = \frac{(Ms - Msd)}{(Msd)} \times 100 \quad (1)$$

Density (ρ) and porosity (P) are crucial factors influencing concrete's functionality and structure. In this study ASTM

C1754 procedures was followed to assess (ρ) and (P). Samples were subjected to a 60 °C oven for 4 days to determine density, with their hardened weight recorded. Apparent porosity (P) was evaluated by submerging samples in water for 24 hours to obtain submerged weight. Calculation of apparent porosity (P) involved using submerged weight, oven-dried weight, volume of water absorbed (Vw), and total specimen volume (V), in accordance with ASTM C1754 guidelines.

$$(P)apparent = \frac{(Vw)}{(V)} \quad (2)$$

The fracture energy (*Gf*) was conducted according to the guidelines published in the JCI-S-001-2003.

Mix	Percentage	Cement (kg/m³)	MK (kg/m³)	Water (kg/m³)	NS (kg/m³)	NA (kg/m³)	SP (kg/m³)
0 MK	0%	390.0	0	175.5	782.4	1037.1	0.221
5 MK	5%	370.5	19.5	175.5	782.4	1037.1	0.395
10 MK	10%	351.0	39.0	175.5	782.4	1037.1	0.207
20 MK	20%	312.0	78.0	175.5	782.4	1037.1	0.273

MK = metakaolin, NS = natural sand, NA = natural aggregate, SP = superplasticizer

Table 3 Mix proportion of concrete containing metakaolin (Concrete mix designs for 1 m³)
3 táblázat Metakaolin tartalmú betonok keverési arányai (beton receptúrák 1 m³-hez)

3. Test results and discussion

Various plots were created to identify and analyze the physical and mechanical properties of concrete, thereby evaluating the effectiveness of metakaolin.

3.1 Apparent Porosity and Density

Apparent porosity (P) is critical for concrete's strength and durability. To measure it, samples were oven-dried, weighed, submerged in water, and re-weighed periodically until saturation. Using dry, saturated, and submerged weights, porosity was calculated. *Fig. 1* shows that increasing metakaolin dosage generally increases porosity, likely due to rapid pozzolanic reactions with $Ca(OH)_2$, producing additional hydration products. Variations in curing conditions and the water-cement ratio also influence porosity. Over time, entrapped water in the concrete matrix is consumed in the pozzolanic reaction, enhancing strength. [11, 12] Study and It was observed that when the metakaolin content was less than 20%, there was a decrease in the overall porosity of the paste. However, when the metakaolin content exceeded 30%, porosity increased, possibly due to the 'filler effect' of fine metakaolin particles and the higher water-to-binder (w/b) ratios associated with increasing metakaolin content. After 100 days of curing, the inclusion of metakaolin led to a reduction in both the pore volume of the mortar and the threshold diameter [13]. Suggests the analysis of the porosity and pore size distribution of cured OPC-metakaolin paste indicates that the incorporation of metakaolin refined the pore structure of the cement paste. Moreover, an increase in metakaolin content resulted in a decrease in the threshold pore size [13]. Also noted that with the increase in the water-to-binder ratio (w/b), the porosity of a paste increases. Hence, it can be deduced that Metakaolin has a more pronounced effect on refining the pore structure of cement pastes at lower w/b ratios in comparison to higher w/b ratios [14]. Also discovered that the incorporation of metakaolin affected the porosity values of pervious mixes, irrespective of aggregate size. With an increase in metakaolin content, porosity values increased linearly, attributed to its filling effect.

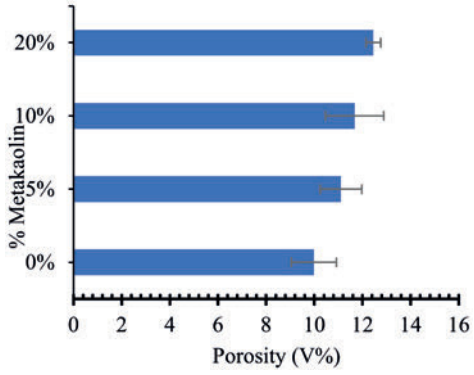

Fig. 1 Apparent porosity of the concrete mixtures
1. ábra Beton keverékek látszólagos porozitása

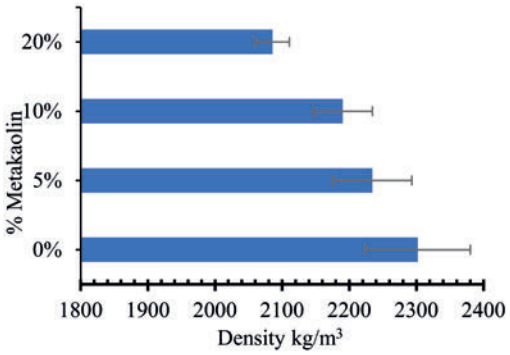

Fig. 2 Metakaolin effect on density of concrete
2. ábra Metakaolin hatása a beton sűrűségére

The density (ρ) of the specimens was determined per ASTM C1688-2014 after 28 days by dividing the dry weight by the volume. Samples were dried for four days, weighed, submerged in water, and their submerged weight recorded. The volume was calculated from the buoyant weight using the density of water. *Fig. 2* shows a significant density decrease with increased metakaolin content, except at 5% dosage, where density was higher than at 10% and 20%. This may be due to metakaolin reacting with calcium hydroxide during cement hydration, forming additional binding material (C-S-H gel). Thus, metakaolin substitution can help produce lightweight concrete [14]. Indicates that the addition of metakaolin had little effect on the concrete density, primarily because of its comparatively small volume in comparison to other ingredients [15]. It has been noted that when the replacement level reaches 20%, the rate of increase in density significantly decreases due to the prevalence of aggregate interlocking.

3.2 Compressive strength

Compressive strength (fc) was measured as the ratio of the failure load supported by the cube specimen to its contact surface area at a constant rate of 0.6 MPa/s. The results, averaged from 4 cube values, were tested at 14, 28, 48, 83, and 90 days. *Fig. 3* shows a significant increase in compressive strength with metakaolin substitution compared to the control mix. At 14, 28, 48, and 90 days, the 5% and 20% metakaolin mixes showed the highest compressive strength, although all replacement percentages performed better than the control mix [13]. Also observed that the pozzolanic reaction exhibited by metakaolin becomes more pronounced with age when substituted at a 5% level, surpassing the reactions seen at 10% and 20% replacement levels. On the other hand, [16] found that the interaction between metakaolin and $Ca(OH)_2$ leads to the formation of additional strength through the production of calcium silicate hydrates (C-S-H). When comparing the compressive strengths (fc) of the cube and half prism specimens, *Fig. 4* displays the interaction plot between the two.

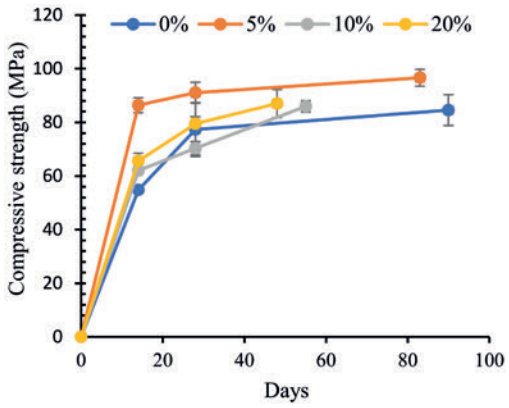

Fig. 3 Compressive strength of concrete cubes
3. ábra Beton kockák nyomószilárdsága

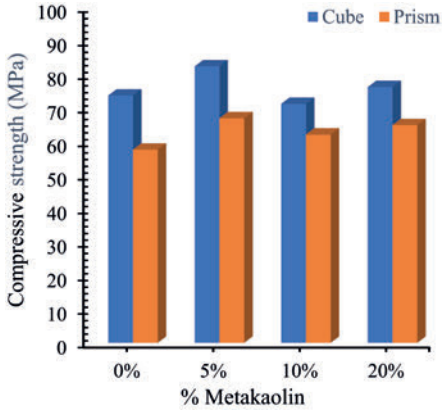

Fig. 4 Compressive strengths of cube and half prism
4. ábra Kocka és félhasáb nyomószilárdsága

From this it can be seen that overall, there isn't a significant difference in the compressive strengths of the cube and half prism specimens; however, on an individual basis, there is a noticeable difference in the compressive strengths of the cube and half prism specimens containing 0% and 5% metakaolin, while the specimens at 10% and 20% have relatively close compressive strengths. This relative rise in compressive strengths could be explained by giving the pozzolanic reaction adequate time to finish. For post-fire residual compressive strength, half prisms were tested after heating to 20 °C to 800 °C in a muffle furnace, following 28 days of natural drying and 4 days at 60 °C to remove moisture. *Fig. 5* and *6* show an initial rise in compressive strength between 200 °C and 300 °C, likely from the hydration of previously unhydrated metakaolin, followed by a rapid decrease after 400 °C, yet still comparable to the control mix. The 5% metakaolin mix maintained good post-fire strength, while the 20% mix showed a significant strength increase at 600 °C. No visible cracks were observed up to 600 °C, with microcracks appearing at 800 °C due to pressure from evaporating water. No spalling occurred, likely due to pre-drying. Maintaining compressive strength at high temperatures is crucial for fire-resistant concrete.

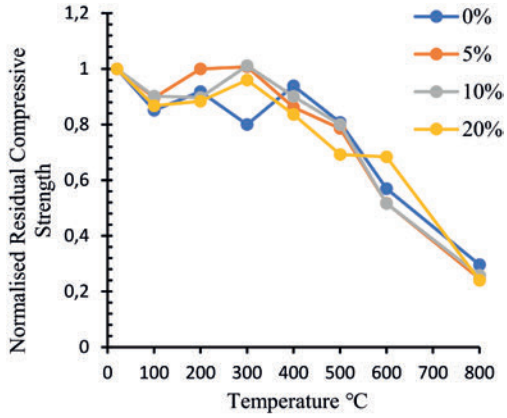

Fig. 5 Effect of temperature on compressive strength
5. ábra Hőmérséklet hatása a nyomószilárdságra

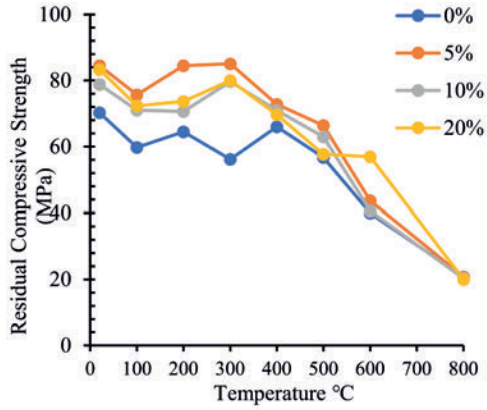

Fig. 6 Effect of temperature on compressive strength
6. ábra Hőmérséklet hatása a nyomószilárdságra

3.3 Flexure tensile strength

Flexural tensile strength test (*fl*) results at 40 days, depicted in *Fig. 7*, shows that higher proportions of metakaolin enhance the flexural tensile strength of the mixes. Notably, 5% and 20% metakaolin mixes demonstrated the most significant improvements compared to the control mix, while the 10% mix showed a decrease, but still better than the control mix, this is attributed to transition where the balance between cement hydration and metakaolin's pozzolanic reaction is less

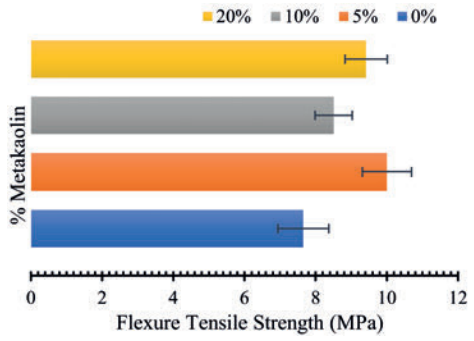

Fig. 7 Metakaolin effect on flexure tensile strength
7. ábra Metakaolin hatása a hajlító húzószilárdságra

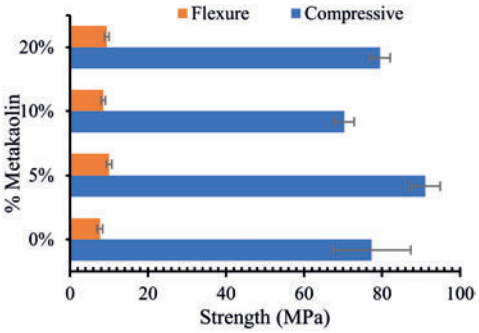

Fig. 8 Comparison of compressive and flexure strengths
8. ábra Nyomószilárdság és hajlító húzószilárdság összehasonlítása

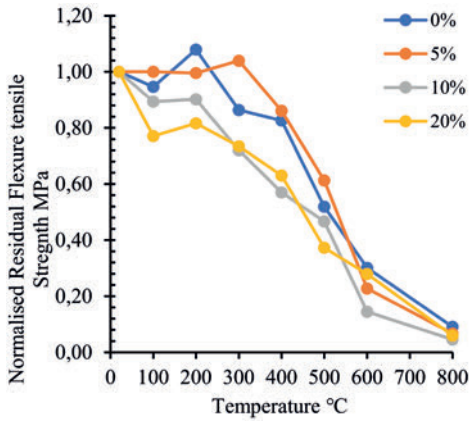

Fig. 9 Effect of temperature on flexure tensile strength
9. ábra Hőmérséklet hatása a hajlító húzószilárdságra

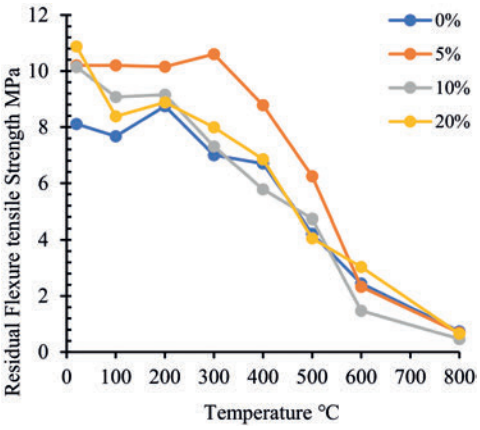

Fig. 10 Effect of temperature on flexure tensile strength
10. ábra Hőmérséklet hatása a hajlító húzószilárdságra

effective. This intermediate content may result in insufficient cement for full hydration while not providing enough metakaolin to enhance pozzolanic activity, leading to a weaker microstructure and poorer bonding between the cement paste and aggregates. *Fig. 8* illustrates that mixes with 5% and 20% metakaolin exhibit significantly higher strengths in both compressive and flexural tensile tests than the control mix, while the 10% metakaolin mix displays a slight decrease in flexural tensile strength and notable reduction in compressive strength compared to the control mix. After 28 days of drying, the impact of metakaolin on concrete's flexural tensile strength at elevated temperatures was assessed. Specimens were heated in an electric muffle furnace from 20 °C to 800 °C. Before the fire test, specimens were dried for approximately 4 days at 60 °C to remove accumulated moisture. *Fig. 9* and *10* show the flexural tensile strength of various mixtures at elevated temperatures, followed by the CMOD test. The flexural tensile strength of the 5% metakaolin mix was comparable to or higher than the control mix and significantly greater than the other mixes, exhibiting a notable increase at 300 °C. However, as the temperature increased further, the flexural strength decreased rapidly, with a slight decrease at 600 °C [17]. Noticed that the sharp increase in flexural tensile strength at 300 °C is primarily attributed to the substantial dehydration of the cement paste.

3.4 Fracture Energy

The fracture energy (*Gf*) was assessed using 72 prisms measuring 70 x 70 x 270 mm each, with a primary crack illustrated in *Fig. 11* [19]. This evaluation encompassed 48 prisms specimens of concrete containing metakaolin in the dosage of 10 and 20% and 24 prisms specimens of concrete without any additive. The fracture energy was determined by analyzing the crack mouth open displacement CMOD-load relationship plots obtained for each test specimen. This energy value was computed using the following equation.

$$Gf = \frac{0.75\,W0 + W1}{A\,lig} \tag{3}$$

$$W1 = 0.75\left(\frac{S}{L}\,m1 + 2m2\right) g.CMODc \tag{4}$$

Where GF - Fracture Energy, W0 - area under CMOD curve until rupture, W1- work done by dead load of jig, Alig – area of the broken ligament, S, L, m1, m2 according [19].

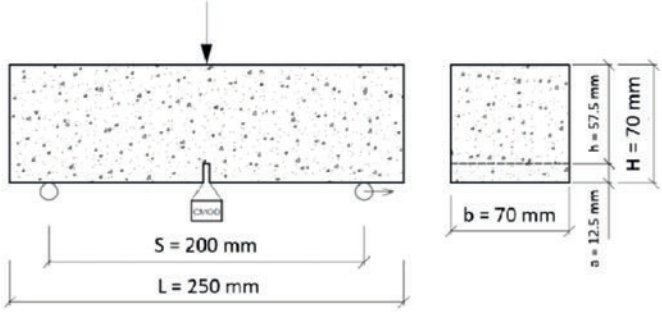

Fig. 11 (CMOD) arrangement [20]
11. ábra (CMOD) kísérleti elrendezés [20]

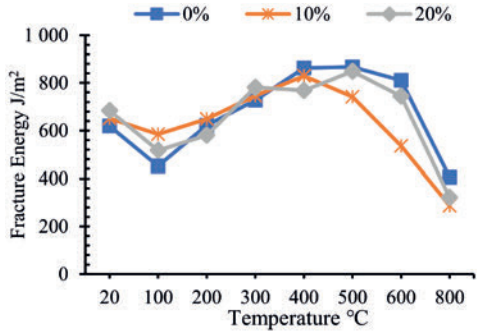

Fig. 12 Temperature effect on fracture energy
12. ábra Hőmérséklet hatása a törési energiára

Fig. 11 shows the modified experimental setup resembling three-point bending tests for flexural tensile strength, featuring a straight notch ending in a U-slot precisely cut at mid-span under point load. Notched three-point bending tests were conducted on each specimen until total failure, recording load-displacement curves at a rate of 0.01 mm/sec under CMOD control. Fracture energy (GF) was estimated by dividing the area under the load-displacement curves. *Fig. 12* displays average CMOD values at load bearing capacity of different mixes, showing a steady increase until reaching peak CMOD, where a slight drop occurred. Notably, a linear decrease in fracture energy was observed for the 10% mix starting from 500 °C, associated with thermal shock from rapid temperature rise. Microcracks in concrete began spreading at 300 °C, while breakdown of calcium hydroxide into calcium oxide and water occurred between 400 °C and 600 °C, peaking at 500 °C. However, over 600 °C, additional deterioration of the C-S-H gel is thought to be the cause of the deterioration of concrete's mechanical and physical characteristics [21]. Since metakaolin's particles are finer than cement's, adding it to the concrete mix can alter the packing density. Increased porosity in the mix leads to the formation of voids and microcracks, which can impact the concentration of stress areas and expedite the initiation and propagation of cracks. These defects lessen the concrete's fracture toughness and weaken it. [21, 22] Observed, the decline in (GF) observed in concrete exposed to heat is attributed to several factor. These include the development of microcracks within the concrete due to high temperatures, alterations in the pore structure, and changes in the existing pore network caused by the release of pore water and weakening of the ITZ (interfacial transition zone) bond due to the breakdown and evaporation of chemical water within the cement paste.

4. Conclusions

Based on the experimental study and observation the following conclusion has been drawn.

- Increasing metakaolin dosage generally increases porosity due to the rapid pozzolanic reaction with calcium hydroxide and changes in paste structure. Variations in curing conditions and water-cement ratio also influenced porosity.
- Density notably decreased with higher metakaolin content, but a slight increase was observed at 5% metakaolin compared to the control mix.
- Metakaolin substitution significantly improved compressive strength, with the greatest enhancement at 5% metakaolin due to rapid pozzolanic reactions and formation of calcium silicate hydrates (C-S-H).
- Flexural strength increased with higher metakaolin proportions; mixes with 5% and 20% showed significant improvements, while at the 10% replacement level, the mix reaches a transitional point where the balance between cement hydration and metakaolin reaction is suboptimal, leading to a reduction in flexure strength but still shows outstanding growth than the control mix.
- Compressive strength of specimens exposed to 20 °C-800 °C initially increased then decreased. Specimens with 5% metakaolin maintained notable post-fire compressive strength, similar to the control mix.
- No spalling was observed during the fire test at high temperatures, likely due to effective pre-test drying, which removed all water content and moisture.
- Concrete mixes with 5% metakaolin demonstrated significant flexural tensile strength compared to the control mix, with a significant increase at 300 °C due to substantial dehydration of the cement paste.
- Fracture energy initially increased linearly with temperature due to improved pore structure, but beyond 500°C, deterioration of the C-S-H gel led to decreased fracture energy.
- The study indicates that metakaolin substitution can enhance concrete's mechanical properties, including compressive and flexural strength, fracture energy, and resistance to water absorption and high temperatures. Mixes with 5% metakaolin showed the most favorable performance, highlighting its practical potential.

Acknowledgements

Project no. PD 146109 has been implemented with the support provided by the Ministry of Culture and Innovation of Hungary from the National Research, Development and Innovation Fund, financed under the OTKA PD_23 funding scheme.

References

[1] C.S. Poon, S. Azhar, M. Anson, Y.L. Wong, Performance of metakaolin concrete at elevated temperatures, Cem Concr Compos 25 (2003) 83–89. https://doi.org/10.1016/S0958-9465(01)00061-0.
[2] A. Borosnyói, A. Szijártó, Metakaolin vizsgálata cement kiegészítő anyagként a k-érték elve szerint, Építőanyag 68 (2016) 40–44. https://doi.org/10.14382/epitoanyag-jsbcm.2016.7.
[3] Z. Shi, Z. Shui, Q. Li, H. Geng, Combined effect of metakaolin and sea water on performance and microstructures of concrete, Constr Build Mater 74 (2015) 57–64. https://doi.org/10.1016/j.conbuildmat.2014.10.023.
[4] P. Duan, Z. Shui, W. Chen, C. Shen, Effects of metakaolin, silica fume and slag on pore structure, interfacial transition zone and compressive strength of concrete, Constr Build Mater 44 (2013) 1–6. https://doi.org/10.1016/j.conbuildmat.2013.02.075.

[5] M.S. Morsy, S.S. Shebl, A.M. Rashad, Effect of fire on microstructure and mechanical properties of blended cement pastes containing metakaolin and silica fume, Silicates Industriels 74 (2009) 59–64.

[6] N. Abdelmelek, N. S. Alimrani, N. Krelias, E. Lubloy, Effect of Elevated Temperatures on Microstructure of High Strength Concrete Based-Metakaolin, Journal of King Saud University - Engineering Sciences (2021). https://doi.org/10.1016/j.jksues.2021.08.001.

[7] F. Cassagnabère, P. Diederich, M. Mouret, G. Escadeillas, M. Lachemi, Impact of metakaolin characteristics on the rheological properties of mortar in the fresh state, Cem Concr Compos 37 (2013) 95–107. https://doi.org/10.1016/j.cemconcomp.2012.12.001.

[8] T.A. Tawfik, K. Aly Metwally, S.A. EL-Beshlawy, D.M. Al Saffar, B.A. Tayeh, H. Soltan Hassan, Exploitation of the nanowaste ceramic incorporated with nano silica to improve concrete properties, Journal of King Saud University - Engineering Sciences 33 (2021) 581–588. https://doi.org/10.1016/j.jksues.2020.06.007.

[9] B. Sabir, S. Wild, J. Bai, Metakaolin and calcined clays as pozzolans for concrete: A review, Cem Concr Compos 23 (2001) 441–454. https://doi.org/10.1016/S0958-9465(00)00092-5.

[10] N. De Belie, M. Soutsos, E. Gruyaert, Properties of Fresh and Hardened Concrete Containing Supplementary Cementitious Materials: State-of-the-Art Report of the RILEM Technical Committee 238-SCM, Working Group 4, 2018.

[11] P. Duan, Z. Shui, W. Chen, C. Shen, Effects of metakaolin, silica fume and slag on pore structure, interfacial transition zone and compressive strength of concrete, Constr Build Mater 44 (2013) 1–6. https://doi.org/10.1016/j.conbuildmat.2013.02.075.

[12] R. Siddique, J. Klaus, Influence of metakaolin on the properties of mortar and concrete: A review, Appl Clay Sci 43 (2009) 392–400. https://doi.org/10.1016/j.clay.2008.11.007.

[13] C.S. Poon, L. Lam, S.C. Kou, Y.L. Wong, R. Wong, Rate of pozzolanic reaction of metakaolin in high-performance cement pastes, Cem Concr Res 31 (2001) 1301–1306. https://doi.org/10.1016/S0008-8846(01)00581-6.

[14] S. Bright Singh, M. Murugan, Effect of metakaolin on the properties of pervious concrete, Constr Build Mater 346 (2022). https://doi.org/10.1016/j.conbuildmat.2022.128476.

[15] N. Saboo, S. Shivhare, K.K. Kori, A.K. Chandrappa, Effect of fly ash and metakaolin on pervious concrete properties, Constr Build Mater 223 (2019) 322–328. https://doi.org/10.1016/j.conbuildmat.2019.06.185.

[16] N. Abdelmelek, E. Lubloy, Evaluation of the mechanical properties of high-strength cement paste at elevated temperatures using metakaolin, J Therm Anal Calorim 145 (2021) 2891–2905. https://doi.org/10.1007/s10973-020-09992-2.

[17] S.I.A. Ali, E. Lublóy, Effect of metakaolin and boron-carbide on the properties of magnetite, basalt and quartz concrete at different elevated temperatures, Constr Build Mater 400 (2023). https://doi.org/10.1016/j.conbuildmat.2023.132593.

[19] Japanese Concrete Institute, Method of test for fracture energy of concrete by use of notched beam, 2 (2003) 1–14.

[20] V. Hlavička, L.E. Hlavicka-Laczák, É. Lublóy, Residual fracture mechanical properties of quartz and expanded clay aggregate concrete subjected to elevated temperature, Constr Build Mater 328 (2022). https://doi.org/10.1016/j.conbuildmat.2022.126845.

[21] A. Sadrmomtazi, S.H. Gashti, B. Tahmouresi, Residual strength and microstructure of fiber reinforced self-compacting concrete exposed to high temperatures, Constr Build Mater 230 (2020) 116969. https://doi.org/10.1016/j.conbuildmat.2019.116969.

[22] P.E. Petersson, Fracture energy of concrete: Practical performance and experimental results, Cem Concr Res 10 (1980) 91–101. https://doi.org/10.1016/0008-8846(80)90055-1.

Ref.:
Yousuf, Zubair – **Hlavička,** Dr. Viktor: *Enhancing Fire Resistance of Concrete through Metakaolin Substitution: A Comprehensive Experimental Study*
Építőanyag – Journal of Silicate Based and Composite Materials, Vol. 76, No. 3 (2024), 101–107 p.
https://doi.org/10.14382/epitoanyag-jsbcm.2024.11

Lignitpernye-alapú geopolimer habok mechanikai tulajdonságainak szabályozása az alapanyag őrlésével

NÉMETH Noémi ▪ Miskolci Egyetem, Műszaki Föld- és Környezettudományi Kar, Nyersanyagelőkészítés és Környezettechnológia Intézet ▪ neno20010702@gmail.com
SZABÓ Roland ▪ Miskolci Egyetem, Műszaki Föld- és Környezettudományi Kar, Nyersanyagelőkészítés és Környezettechnológia Intézet ▪ roland.szabo@uni-miskolc.hu
DEBRECZENI Ákos ▪ Miskolci Egyetem, Műszaki Föld- és Környezettudományi Kar, Bányászat és Energia Intézet ▪ akos.debreczeni@uni-miskolc.hu
MUCSI Gábor ▪ Miskolci Egyetem, Műszaki Föld- és Környezettudományi Kar, Nyersanyagelőkészítés és Környezettechnológia Intézet ▪ gabor.mucsi@uni-miskolc.hu

Érkezett: 2024. 07. 02. ▪ Received: 02. 07. 2024. ▪ https://doi.org/10.14382/epitoanyag-jsbcm.2024.12

Abstract

The present study investigates the mechanical properties (compressive and flexural strength), density, and porosity of environmental-friendly, porous geopolymer composites or geopolymer foams. Geopolymer foams can be obtained by several different foaming methods, the most common being direct foaming. During the process of direct foaming a so-called foaming/blowing agent is introduced to the geopolymer slurry which creates gas bubbles, and pores. The properties of geopolymer foams generally depend on their pore structure, which is defined by several factors - grinding fineness, L/S ratio, and foaming agent. To optimise these factors the authors of this paper carried out a systematic experiment on geopolymer foam specimens made of lignite fly ash (milled for 15, 30, and 60 minutes in a laboratory ball mill) and metakaolin, with H_2O_2 as a chemical foaming agent. The most homogeneous pore structure could be achieved with 2 wt.% H_2O_2 and 15 minutes of mechanical activation. Even though the 60-minute milling time caused large, inhomogeneous pores it resulted in the maximum compressive (12,90 MPa) and flexural strength (4,88 MPa), and the lowest porosity value (26,2 v/v%).

Keywords: Lignite fly ash, mechanical activation, geopolymer foam, compressive strength, flexural strength, density, porosity
Kulcsszavak: Lignitpernye, mechanikai aktiválás, geopolimer hab, nyomószilárdság, hajlítószilárdság, testsűrűség, porozitás

NÉMETH Noémi
A Miskolci Egyetem Műszaki Föld- és Környezettudományi Karának harmadéves, nyersanyag-előkészítés specializáción tanuló BSc hallgatója. A 36. OTDK Műszaki Tudományi Szekció – Környezetmérnöki Tudomány 3. Tagozat - első helyezettje. Pályamunkájának címe: Hulladék alapú szálerősített geopolimer kompozitok eljárástechnikai vizsgálata.

SZABÓ Roland
A Miskolci Egyetem Nyersanyagelőkészítés és Környezettechnológia Intézetének tudományos munkatársa, okl. előkészítéstechnikai mérnök. PhD fokozatát 2020-ban szerezte a Miskolci Egyetemen. Fő kutatási területe: szilikátalapú ipari hulladékok hasznosítási lehetőségének vizsgálata geopolimerek előállítására, különös tekintettel a habszerkezetű termékek fejlesztésére.

DEBRECZENI Ákos
A Miskolci Egyetem Bányászati és Geotechnikai Intézeti Tanszék vezetője (2010-), egyetemi docens, okleves bányamérnök. Fő szakmai kompetenciái: bányászat, bányagépészet, geotechnika, kőzetmechanika. 2012-től az MTA Bányászati Tudományos Bizottság, Bányászati, Geotechnikai és Nyersanyagelőkészítési Albizottság elnöke.

MUCSI Gábor
20 éve foglalkozik a környezetipar, fenntarthatóság kérdéseihez kapcsolódó oktatási, valamint kutatás-fejlesztési és innovációs feladatokkal. Kutatási területe a szilárd hulladékok előkészítése és hasznosítása, az ipari hulladékok (salakok, pernyék, építési hulladék) mechanikai aktiválása reaktivitásuk szabályozása érdekében, geopolimerek fejlesztése, hulladékok szinergikus hasznosítása. 2020-tól a Miskolci Egyetem Műszaki Föld- és Környezettudományi Karának dékánja. Szilikátipari Tudományos Egyesület Cement Szakosztályának elnöke.

1. Bevezetés

A beton előállításához elengedhetetlen cement gyártásának világszintű CO_2 -kibocsátása 2021-ben 2,9 milliárd tonna volt – ez a teljes globális CO_2 emisszió körülbelül 7%-át jelentette. A cement iránti folyton növekvő kereslet kielégítése, ugyanakkor a cementipar jelentős karbonlábnyomának csökkentése az eddigi tendenciák szerint nem tűnik effektíven összeegyeztethetőnek. Az Európai Unió a European Green Deal-ben („Európai Zöld Megállapodás") megfogalmazta klímasemlegességi irányelveit és célkitűzéseit, a European Climate Law („Európai Klímarendelet") pedig jogi szintre emelte ezeket. Ennek értelmében az EU és tagállamai kötelezettséget vállaltak az üvegházhatású gázok kibocsátásának legalább 50%-kal történő csökkentésére 2030-ig (1990-es értékekhez képest), illetve a nulla nettó kibocsátás („net zero emission") elérésére 2050-ig [1, 2, 3].

A cementgyártás során kibocsátott CO_2 50-60%-a a mészkő kalcinálása, a klinker előállítása során, 30-40% a kalcináláshoz, termikus reakciókhoz szükséges hőenergia előállítása során, 10%-a pedig az villamosenergia felhasználása, valamint a cement szállítása során keletkezik [2, 3]. Ebből az következik, hogy a CO_2 emisszió effektív redukálása egyrészt a cementben található klinker egy részének például kohósalakkal, pernyével, természetes puccolánnal történő helyettesítésével (CEM II, CEM III), a gyártási folyamathoz szükséges magas hőmérséklet (1200-1450 °C) csökkentésével, a hőenergia-veszteség minimalizálásával és a hulladék-hő visszanyerésével (waste heat recovery), a hőenergia környezetbarát/megújuló energiahordozókból történő előállításával, a szén-dioxid leválasztás-, hasznosítás-, és tárolás (Carbon capture, utilization and stabilization) technológia alkalmazásával, illetve alacsony karbonkibocsátású alternatív cementek/kötőanyagok széleskörű elterjedésével lehetséges, amelyek életciklusuk során több szén-dioxidot kötnek meg, mint amennyi előállításuk során keletkezik [2].

A geopolimerek szervetlen polimer-szerkezetű alternatív, környezetbarát kötőanyagok, amelyek szilárd-aluminoszilikátok lúgos (ritkábban savas) közegben végbemenő reakciója, az ún. geopolimer szintézis során keletkeznek alacsony hőmérsékleten (30-100 °C) [4, 5, 6]. A geopolimerek előállításához alkalmazható szilárd, magas alumínium-, és szilíciumtartalmú prekurzorok többek között a kaolin, metakaolin, zeolitok, szilikapor, erőműi pernye, vörösiszap, kohósalak, rizshéj hamu, betontörmelék, bányászati meddő és téglatörmelék [4, 5, 6, 7]. A felsorolt alapanyagok túlnyomó része olyan nagy mennyiségben keletkező ipari hulladék, amelyek biztonságos tárolása komoly költségekkel és környezeti kockázatokkal jár. A leggyakrabban alkalmazott lúgos kémhatású aktiváló oldatok a NaOH, Na_2SiO_3, KOH, K_2SiO_3 [8], a ritkábban használt savas kémhatású aktiváló oldatok a H_3PO_4, $AlPO_4$, illetve a termész-

tes eredetű humin sav [4]. A geopolimerek rendkívül gyorsan kötnek, a bekeveréstől számított 4 órát követően képesek végleges szilárdságuk 70%-át elérni [8]. A geopolimerek ezen kívül kiváló termikus stabilitással rendelkeznek, térfogati- és lineáris zsugorodásuk kisebb, mint a portlandcement esetén; hő-és tűzállóak, valamint a kémia korrózióval szemben is ellenállónak bizonyultak [8, 9]. A geopolimerek nyomó-, valamint hajlítószilárdsága képes felvenni a versenyt a hagyományos cementek szilárdságával, amennyiben optimalizáljuk az anyagi-, és külső környezeti paramétereket, amelyeket az *1. ábra* szemléltet [9]. Ezen tulajdonságoknak köszönhetően a geopolimerek ígéretesek lehetnek az építőiparban (cementek, út- és járdarétegek, falazó- és szigetelő téglák, különleges hő- és tűzálló bevonatok, burkolatok), és a környezetvédelemben (nehézfémekkel szennyezett vizek szűrése, adszorbensek) [4, 7].

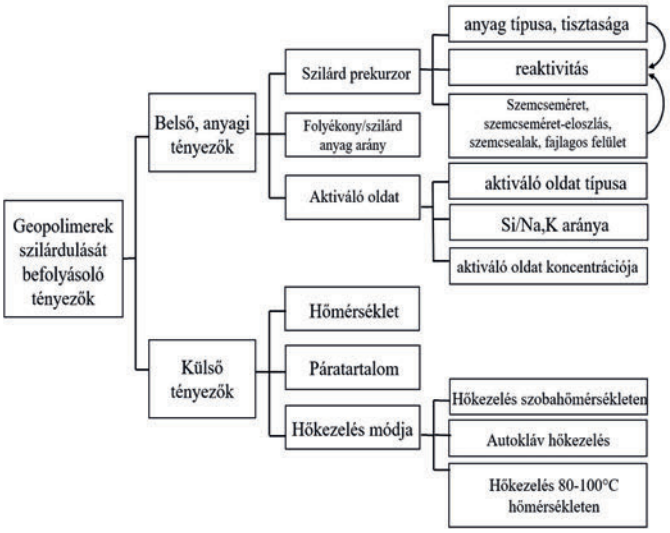

1. ábra A geopolimereket szilárdságát befolyásoló külső és belső, anyagi tényezők [9]
Fig 1. Internal and external factors of the hardening properties of geopolymers [9]

A geopolimerekből a legkülönbözőbb fizikai és kémiai habképző eljárásokkal állíthatunk elő porózus, habszerkezetű geopolimer kompozitokat. A leggyakrabban alkalmazott habosítási módszerek a közvetlen, vagy direkt habosítás („direct foaming"), a replikációs módszer („replica method"), az ideiglenes töltőanyag módszer („sacrificial filler method"), és az additív gyártási technológia („additive manufacturing") [10, 11, 12]. A felsorolt eljárások között a legelterjedtebb a közvetlen habosítás, mely lényege, hogy a folyékony, homogén geopolimer zagyba az ún. habképző reagensek bomlásával gázt (például H_2, O_2) juttatunk. Az így keletkező nedves hab megszilárdul; a folyamat végterméke a porózus szerkezetű, szilárd geopolimer hab [12]. A habképző reagensek lehetnek különböző fémporok (például: alumínium-, cink por [12, 13]), fémötvözetek (például: szilícium-karbid, ferroszilícium [12]), továbbá lehet nátrium-hipoklorit (NaOCl), nátrium-perborát és hidrogén-peroxid (H_2O_2) [12, 13]. Az egyes habképző reagensek eltérő reakciói, eltérő méretű, alakú pórusokat, pórusszerkezetet eredményeznek, amely meghatározza a geopolimer hab tulajdonságait (szilárdság, sűrűség, porozitás) [14]. Számos kutatás rámutatott, hogy a hidrogén-peroxid például inhomogén, gyakran nyílt pórusszerkezetet eredményez, mert bomlása lúgos környezetben instabil, és a keletkező gázbuborékok mérete a koaleszcencia következtében megnő [11, 12, 14, 15]. Ez a jelenség a megnöveli a geopolimer habok porozitását, ám sűrűségét csökkenti, és ezáltal rontja mechanikai tulajdonságait [16]. A geopolimer hab pórusszerkezetét meghatározza továbbá a geopolimer paszta reológiája és viszkozitása, amelyeket legfőképpen a folyékony/szilárd anyag arány (L/S arány) és az aluminoszilikát prekurzor őrlési finomsága befolyásol [13, 17].

Jelen kutatás célja a közvetlen habosítással előállított, lignitpernye-alapú habszerkezetű geopolimerek mechanikai tulajdonságainak vizsgálata, valamint optimalizálása a pernye őrlési finomságának és a habosítószer (H_2O_2) adagolásának változtatásával. A kutatás kezdeti-, előkísérleti fázisában elvégeztünk egy kétlépcsős kísérletsorozatot, amelyben az előbb felsorolt két paraméter geopolimer paszta, és hab tulajdonságaira – bedolgozhatóság, folyási tulajdonság, kötési idő, pórusméret, pórusszerkezet – gyakorolt hatásait vizsgáltuk hengeres próbatesteken. Elsőként az őrlési finomság, majd a H_2O_2 mennyisége által előidézett változásokra fókuszáltunk. Ezután az előkísérletek tapasztalatai alapján megválasztott keverési paraméterekkel elkészített szabványos méretű (160 × 40 × 40 mm) próbatestek hajlító-, és nyomószilárdságát, testsűrűségét, illetve porozitását vizsgáltuk.

2. Anyagok és módszerek

A geopolimer próbatestek előállításához metakaolint (MK), valamint a MVM Mátra Energia Zrt.-nél keletkező lignit pernyét alkalmaztunk. A nyers pernye fő oxidos komponenseinek tömegszázalékos mennyiségei a következők voltak: SiO_2 (47,90%), Al_2O_3 (16,53%), Fe_2O_3 (11,15%), CaO (11,41%), MgO (2,87%), S (3,38%). A pernye izzítási vesztesége 3,66% volt. A pernyét 15, 30, illetve 60 perces mechanikai aktiválásnak vetettük alá laboratóriumi golyósmalomban (Ø305×305 mm).

A szilárd anyag 85 m/m%-ban tartalmazta a különböző pernyeőrleményeket és 15 m/m%-ban a metakaolint. Aktiváló oldatként 8 M NaOH-ot és Geosil 14517 típusú vízüveget alkalmaztunk 1:1 arányban. A geopolimerek habosításához 30 %-os H_2O_2-ot használtunk. A geopolimer hab próbatestek tulajdonságait (nyomó- és hajlítószilárdság, testsűrűség, porozitás) 7, illetve 28 napos korban vizsgáltuk. A *2. ábra* az elkészítés folyamatát mutatja be. Minden összetétel esetén 3 próbatest készült.

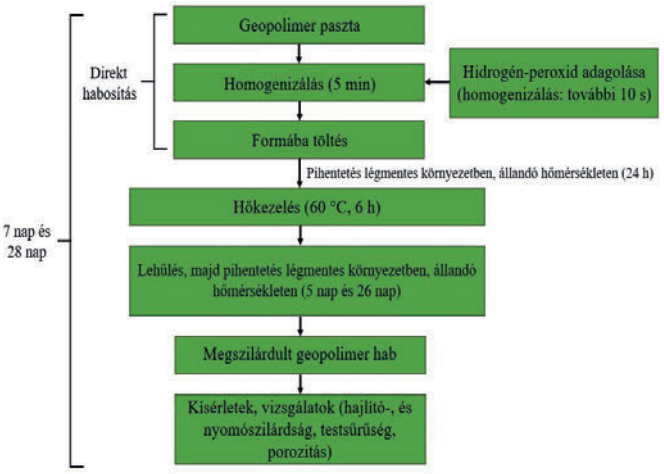

2. ábra A geopolimer hab próbatestek előállításának folyamata
Fig. 2 Preparation process of geopolymer foam specimens

3. Eredmények

3.1 Pernye mechanikai aktiválása

A nyers pernye, a pernye őrlemények és a metakaolin szemcseméret-eloszlásának meghatározására Horiba LA-950V2 típusú lézeres szemcseméret-elemzőt alkalmaztunk. A minták nevezetes szemcseméreteit (x_{10}, x_{50}, x_{80}), valamint fajlagos felületüket az *1. táblázat* tartalmazza.

	Fajlagos felület (cm^2/cm^3)	x_{10} (μm)	x_{50} (μm)	x_{80} (μm)
Nyers pernye	1249,7	20,02	96,43	173,85
15 min	2523,5	9,73	47,69	94,97
30 min	5201,3	5,40	17,04	36,04
60 min	10833,0	3,40	14,56	30,69
MK	39051,0	0,33	6,09	8,73

1. táblázat Az alapanyagok fajlagos felülete és nevezetes szemcseméreteik
Table 1. Specific surface area and characteristic particle size values of the raw materials

Az őrlési idő növelésével jelentősen lecsökkent az őrlemények szemcsemérete, és növekedett az őrlemények fajlagos felülete. Már 15 perc őrlést követően a felére csökkent a pernye medián szemcsemérete (x_{50}) – 96,43 µm-ről 47,69 µm-re. 30 perc őrlés után már nem történt jelentős szemcseméret-csökkenés, azonban a 60 percig őrölt pernye fajlagos felülete (10833,0 cm^2/cm^3) a 30 perces őrlemény kétszerese (5201,3 cm^2/cm^3) volt. Ez a jelenség a szubmikronos mérettartományú finomszemcsék megjelenésével és megnövekedett mennyiségével magyarázható.

3.2 Előkísérletek eredményei

Az előkísérletek első fázisában a pernye őrlési finomságának hatását vizsgáltuk L/S=0,74 arány (42,5% aktiváló oldat/57,5% szilárd anyag) mellett 3 m/m% H_2O_2 [13] habosítószer adagolásával. A geopolimer pasztákat minden esetben megfelelően be lehetett keverni ám a 30, illetve 60 perces pernyeőrleményekből előállított paszták bedolgozhatósága csökkent, ugyanis a kötés már a formába töltés során megkezdődött. Ebből adódóan a teljesen megszilárdult próbatestek egy részén az anyag rétegződését figyeltük meg. A 30 és 60 perces őrleményekből készült keverékek rendkívül hevesen reagáltak a H_2O_2 -dal. A habosodás azonnal, még a H_2O_2 bekeverése (amely mindösszesze 10 másodperc volt) közben megkezdődött, erős gázfejlődés kíséretében, és a formába töltés során teljesen végbement – ez gyártástechnológiai szempontból rendkívül előnytelen. Ezt a jelenséget a nyers pernye, valamint a 15 perces őrlemény használata során nem tapasztaltuk, itt a habosodás ideálisan, a formába töltés után kezdődött meg és ment végbe. Az intenzív habosodás oka feltételezhetően a pernye összetételével és az őrlés hatására megnövekedett fajlagos felülettel hozható kapcsolatba, azonban ennek megállapítására mélyrehatóbb vizsgálatok szükségesek. A 30 és 60 perces őrleményt tartalmazó próbatestek pórusainak mérete rendkívül széles tartományban változott, a mikro-, és makropórusok egyaránt jellemezték a hab pórusszerkezetét. A leghomogénebb pórusszerkezetet a 15 perces pernyeőrleményből készült próbatestek esetén tapasztaltuk (*3. ábra*).

A második előkísérlet során a H_2O_2 pórusszerkezetre gyakorolt hatását vizsgáltuk a habosítószer 1, 2, 3, illetve 5 m/m%-ban való adagolása mellett. A H_2O_2 mennyisége a keletkező pórusok méretével és a pórusszerkezet inhomogenitásával egyenes arányosságot mutatott. A vizsgált koncentrációk közül a 2 m/m/%-os H_2O_2 tartalmat találtuk optimálisnak, mind a pórusméretet, mind a pórusszerkezet homogenitását figyelembe véve (*3. ábra)*, továbbá az első kísérletben 3m/m% mellett megfigyelt heves gázfejlődés is mérséklődött.

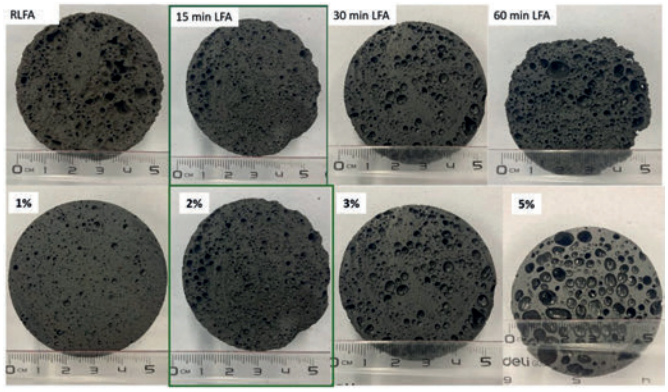

3. ábra Az őrlési finomság (felső sor) és a H_2O_2 adagolásának (alsó sor) hatása
Fig. 3 The effect of grinding fineness (upper row) and the addition of H_2O_2 (lower row)

3.3 Hajlítószilárdság vizsgálat eredményei

A geopolimer hab próbatestek hajlítószilárdság-testűrűség diagramját a *4. ábra* mutatja be. Az ábra alapján megállapítható, hogy a mechanikai aktiválás által jelentősen megnövelt őrlési finomság és fajlagos felület a próbatestek hajlítószilárdságára kedvezően hatottak. A 60 percig őrölt pernyéből készült próbatestek hajlítószilárdsága 7 napos korban 127%-kal (3,77 MPa), míg 28 napos korban 98%-kal (4,88 MPa) nagyobb értéket mutatott, mint a nyers pernyéből készült próbatesteké (1,66 és 2,47 MPa 7 és 28 napos korban).

A nagyobb őrlési finomság alapvetően tömörebb geopolimer szerkezetet, mátrixot eredményezett, így a nagyméretű pórusok és az inhomogén pórusszerkezet ellenére is nagyobb sűrűségű próbatestek készültek a finomabb szemcsézetű pernyeőrleményekből. Szabó és mtsai. szerint [13] ez azzal magyarázható, hogy a pernye őrlési finomságának növelése csökkenti a geopolimer paszta viszkozitását, és egy adott L/S aránynál (0,82) és fajlagos felületérték (3000 cm^2/g) fölött a paszta reológiát vált (Bingham-plasztikusból Newtoni folyási viselkedésűvé változik), amelynek eredményeként a habosodást okozó gázok könnyen eltávozhatnak a pasztából, tömörebb geopolimer habot eredményezve. Hasonló jelenség figyelhető meg a *4. ábrán* is, melynél az látszik, hogy kezdetben az őrlési finomság növelése segítette a paszta habosodását (melyet a csökkenő sűrűség is alátámaszt). Ugyanakkor, 30 és 60 perces őrlemény használata során feltételezhetően a paszta megváltozott (Newtoni) folyási viselkedésének köszönhetően a sűrűség növekedése tapasztalható, amelynek eredményeként a hajlítószilárdság értéke is nőtt.

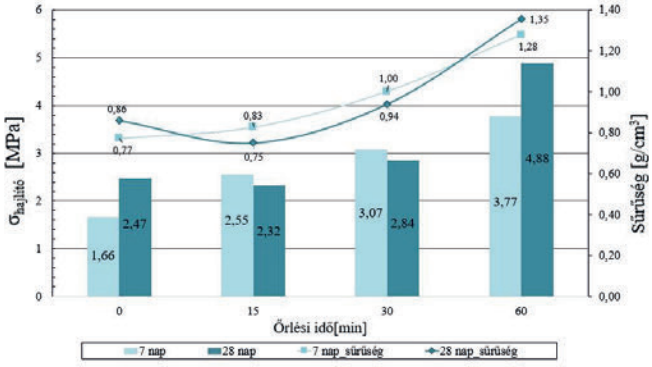

4. ábra A geopolimer hab próbatestek hajlítószilárdság és testsűrűség értékei
Fig. 4 The flexural strength and density values of geopolymer foam specimens

3.4 Nyomószilárdság vizsgálat eredményei

A hajlítószilárdság vizsgálat során kettétört próbatesteken elvégzett nyomószilárdság vizsgálat eredményeit, illetve a geopolimer habok testsűrűségét az *5. ábra* mutatja be. A nyomószilárdság eredmények is igazolják, hogy a nagyobb sűrűségű próbatestek mechanikai tulajdonságai jobbnak bizonyultak, mint a kisebb sűrűségű próbatesteké. A pernye mechanikai aktiválásának eredményeként a 60 perces őrlemény használata kiugró nyomószilárdsághoz (12,91 MPa) vezetett 28 napos korban, amely még a 30 perces őrleményből készült geopolimer hab szilárdságához képest is 207%-os növekedést mutat.

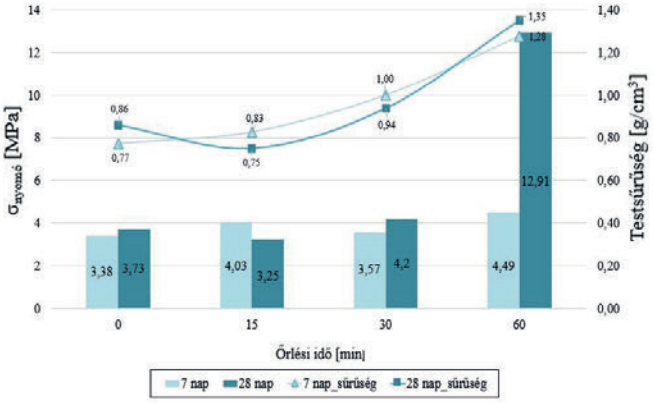

5. ábra A geopolimer hab próbatestek nyomószilárdság és testsűrűség értékei
Fig. 5 The compressive strength and density values of geopolymer foam specimens

3.5 Porozitás

A porozitás vizsgálat eredményei jól követik a próbatestek testsűrűség-változását. A *6. ábrán* látható, hogy az optimálisnak ítélt 15 perces őrleményből készült próbatestek porozitása mutatta a legnagyobb értéket (52,5 V/V%), míg a legjobb mechanikai tulajdonságokkal rendelkező, 60 perces őrleményből készült próbatestek porozitása 26,2 V/V%. Ez is alátámasztja Szabó és mtsai [13] azon megállapítását, miszerint egy adott L/S aránynál a pernye finomsága jelentős hatással van a geopolimer paszta habosodására, ezáltal a geopolimer poózus szerkezetének kialakulására, mivel a mechanikailag aktivált pernyéből – a megváltozott folyási viselkedés következtében – tömörebb, mikropórusoktól mentes geopolimer mátrixot lehet előállítani. Ugyanakkor a kisméretű pórusok egyesülve nagyobb méretű pórusokat hoznak létre, amelyek főként a habosított geopolimer felső részén koncentrálódnak inhomogén pórusszerkezetet eredményezve.

A geopolimer hab próbatestek porozitás értékeit a *6. ábra* mutatja be.

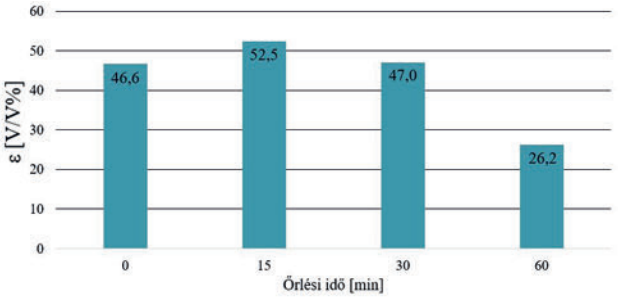

6. ábra Próbatestek porozitásának változása az őrlési finomság növelésével
Fig. 6 Porosity of geopolymer foam specimens with increasing grinding fineness

4. Konklúzió

A lignitpernye mechanikai aktiválásával nagymértékben csökkenthető annak szemcsemérete és jelentősen növelhető fajlagos felülete. A mechanikai aktiválás eredményeként megnövekszik a pernye reaktivitása, ami a geopolimer szintézis szempontjából előnyös, hiszen az előállított geopolimer mátrixa tömörebb és kevesebb mikropórust tartalmaz. Ugyanakkor a habosított geopolimerek előállításánál a habosító/habképző reagens – H_2O_2 – adagolása során ez a nagyfokú reaktivitás nem bizonyult előnyösnek, mivel a 30 és 60 percig őrölt pernyéből készült habokban keletkező gázbuborékok koaleszcenciáját eredményezte, amely a megszilárdult habokban nagyméretű, inhomogén pórusokat eredményezett. A leghomogénebb pórusszerkezete a 15 perces pernyeőrleményből készült próbatesteknek volt, az optimalizált 2 m/m%-os H_2O_2 tartalom mellett.

A geopolimer habok mechanikai tulajdonságai (hajlító-, és nyomószilárdság) az őrlési finomsággal és a testsűrűséggel egyenes arányosságban, míg a porozitással fordított arányosságban állnak. A legnagyobb hajlító-, és nyomószilárdság értékeket (4,88 MPa és 12,91 MPa), valamint a legkisebb porozitást (16,2 V/V%) a 60 perces őrleményből előállított próbatestek mutatták.

Köszönetnyilvánítás

Jelen kutatómunka a Kulturális és Innovációs Minisztérium ÚNKP-23-1 kódszámú Új Nemzeti Kiválósági Programjának a Nemzeti Kutatási, Fejlesztési és Innovációs Alapból finanszírozott szakmai támogatásával készült.

Irodalomjegyzék

[1] United Nations Environment Programme (2022). 2022 Global Status Report for Buildings and Construction: Towards a Zero-emission, Efficient and Resilient Buildings and Construction Sector. Nairobi
[2] Supriya, R. Chaudhury, U. Sharma, P.C. Thapliyal, L.P. Singh, (2023) Low-CO2 emission strategies to achieve net zero target in cement sector, Journal of Cleaner Production, Vol. 417, 137466, ISSN 0959-6526, https://doi.org/10.1016/j.jclepro.2023.137466.
[3] Marmier, A.(2023) Decarbonisation options for the cement industry, EUR 31378 EN, Publications Office of the European Union, Luxembourg, ISBN 978-92-76-61599-6, https://doi.org/10.2760/174037.

[4] Krishna, R. S., Mishra, J., Zribi, M., Adeniyi, F., Saha, S., Baklouti, S., Gökçe, H. S. (2021). A review on developments of environmentally friendly geopolymer technology. Materialia, 20, 101212, https://doi.org/10.1016/j.mtla.2021.101212.

[5] Matsimbe, J.; Dinka, M.; Olukanni, D.; Musonda, I. (2022). Geopolymer: A Systematic Review of Methodologies. Materials 2022, 15, 6852, https://doi.org/10.3390/ma15196852.

[6] Shehata, N., Ali, E. T. S., Abdelkareem, M. A. (2020). Recent progress in environmentally friendly geopolymers: A review. Science of The Total Environment. Vol. 762, March 2021, 143166, https://doi.org/10.1016/j.scitotenv.2020.143166.

[7] Cong, P., Cheng, Y. (2021). Advances in geopolymer materials: A comprehensive review. Journal of Traffic and Transportation Engineering (English Edition). Vol. 8, June 2021, pp. 283-314, https://doi.org/10.1016/j.jtte.2021.03.004.

[8] Burduhos Nergis, D. D., Abdullah, M. M. A. B., Vizureanu, P., Tahir, M. F. M. (2018). Geopolymers and Their Uses: Review. IOP Conference Series: Materials Science and Engineering. 374, 012019, https://doi.org/10.1088/1757-899x/374/1/012019.

[9] Zhao, J., Tong, L., Li, B., Chen, T., Wang, C., Yang, G., Zheng, Y. (2021). Eco-friendly geopolymer materials: A review of performance improvement, potential application and sustainability assessment. Journal of Cleaner Production. Vol. 307, July 2021, 127085, https://doi.org/10.1016/j.jclepro.2021.127085.

[10] Zhang, X., Bai, C., Qiao, Y., Wang, X., Jia, D., Li, H., Colombo, P. (2021). Porous geopolymer composites: A review. Composites Part A: Applied Science and Manufacturing, Vol. 150, November 2021, 106629, https://doi.org/10.1016/j.compositesa.2021.106629.

[11] Li, X., Bai, C., Qiao, Y., Wang, X., Yang, K., Colombo, P. (2022) Preparation, properties and applications of fly ash-based porous geopolymers: A review. Journal of Cleaner Production, Vol. 359, July 2022, 132043, https://doi.org/10.1016/j.jclepro.2022.132043.

[12] Bai, C., Colombo, P. (2018) Processing, properties and applications of highly porous geopolymers: A review. Ceramics International, Vol. 44, pp. 16103-16118, https://doi.org/10.1016/j.ceramint.2018.05.219.

[13] Szabó, R., Gombkötő, I., Svéda, M., Mucsi, G. (2017). Effect of Grinding Fineness of Fly Ash on the Properties of Geopolymer Foam. Archives of Metallurgy and Materials. Vol. 62(2), pp. 1257–1261, https://doi.org/10.1515/amm-2017-0188.

[14] V. Ducman, L. Korat. (2016) Characterization of geopolymer fly-ash based foams obtained with the addition of Al powder or H2O2 as foaming agents. Materials Characterization. Vol. 113, pp. 207-213, https://doi.org/10.1016/j.matchar.2016.01.019.

[15] Boros, A., Korim, T. (2022) Development of Geopolymer Foams for Multifunctional Applications. Crystals. Vol. 12, No. 3, March 2022, 386, https://doi.org/10.3390/cryst12030386.

[16] Rizal, F., Pratama, A. P., Khamistan, Fauzi, A., Syarwan, Azka, A. (2020). Effect of H2O2 as the Foaming Agent on the Geopolymer Mortar using Curing of Room Temperature. IOP Conference Series: Materials Science and Engineering. Vol. 854, 012022, https://doi.org/10.1088/1757-899X/854/1/012022.

[17] Szabó, R., Mucsi, G. (2015). Generally About Geopolymer Foams. https://doi.org/10.26649/musci.2015.014.

Ref.:
Németh, Noémi – **Szabó**, Roland – **Debreczeni**, Ákos – **Mucsi**, Gábor: *Lignitpernye-alapú geopolimer habok mechanikai tulajdonságainak szabályozása az alapanyag őrlésével*
Építőanyag – Journal of Silicate Based and Composite Materials, Vol. 76, No. 3 (2024), 108–112 p.
https://doi.org/10.14382/epitoanyag-jsbcm.2024.12

The silica-alkaline reaction of aggregates is more realistic than the alkaline-carbonate reaction of aggregates

Reham Abu-Elwafa MOHAMED
Researcher in raw building material chemistry and technology in Housing and Building National and Research Center (HBNRC), Cairo, Egypt

Sayeada Rawwash ZEEDAN
Professor in raw building material chemistry and technology in Housing and Building National and Research Center (HBNRC), Cairo, Egypt

Reham Abu-Elwafa MOHAMED ▪ Housing and Building National and Research Center (HBNRC), Egypt ▪ rehamabuelwafa@gmail.com

Sayeada Rawwash ZEEDAN ▪ Housing and Building National and Research Center (HBNRC), Egypt ▪ zeedansun@yahoo.com

Érkezett: 2024. 09. 26. ▪ Received: 26. 09. 2024. ▪ https://doi.org/10.14382/epitoanyag-jsbcm.2024.13

Abstract
The main objective of this research is shedding light on the siliceous and carbonate reactions. Is the use of alkali-silica reactions suitable for aggregates containing limestone? Alkali-silica reaction (ASR) and the related deformation are significant issues with concrete construction durability that date back to the 1940s. This harmful reaction results in excessive expansion and fissures, which can seriously damage concrete structures. Understanding the ASR mechanism is still difficult because of complicating processes and reactions, despite long-standing observation and several ASR investigations. Therefore, the alkali mortar bar test was carried out for five samples containing limestone and dolomitic stone so that it could obtain results within 56 days, compared to obtaining results in 360 days by using the carbonate alkaline reaction test. In this study, the alkali mortar bar test and the alkali carbonate test were determined on three limestone samples and two dolomitic stone samples. Casting of mortar bars with the specified aggregate (2.36 mm- 150 μm), cured in 1 N of sodium hydroxide solution at 80 °C and a concrete prism of alkali carbonate reaction with aggregate of (19 mm - 12.5 mm), stored at 38°C over water. The accelerated mortar bar reaction gave a higher rate of expansion in a short period than the carbonate reaction, although the carbonate reaction proved that the aggregate was reactive after a long period and it was not exposed to high temperature and sodium hydroxide solution. The results showed that the accelerated mortar bar reaction gave a higher rate of expansion in a short period than the carbonate reaction, although the carbonate reaction proved that the aggregate was reactive after a long period and it was not exposed to high temperature and sodium hydroxide solution. The results of the accelerated mortar bar test and the alkali-carbonate test were applied to SEM analysis, which confirmed that calcite and brucite were produced as a result of the reaction between the lime stone and dolomite crystals and the alkali content in the cement.
Keywords: alkali silica reaction, alkali carbonate reaction, expansion, mortar bar, concrete prism
Kulcsszavak: alkáli-szilikát reakció, alkáli-karbonát reakció, duzzadás, habarcs hasáb, beton hasáb

1. Introduction

By creating concrete mixtures that minimize reaction harm and creating technologies to reduce the negative effects of negative expansion in existing buildings, it is essential to have a thorough understanding of the ACR technique in order to choose the best method for mitigating negative growth in new concrete structures. Despite the fact that these ACR and ASR cause concrete to degrade in similar ways, the reaction products that distress the concrete are different from one another, according to the knowledge currently available (ASR gel for ASR vs. brucite formation for ACR). The major several accepted theses that describe how ACR works and how aggregates expand as a result: (1) expansion-free dedolomitization (Swenson & Gillott, 1964); and (2) dedolomitization-induced increase (Hadley, 1964a, Tang et al., 1987; Ozol,1994), 3) Katayama's Alkali Silica Reaction (Katayama, 2010; Gr (Fecteau et al., 2012) and (4) The alkali-silica reaction (ASR), which happens in cementitious materials, is caused when siliceous aggregate particles mix with alkali-sodium and alkali-potassium created during Portland cement hydration. When pore fluid is absorbed, a gelatinous substance is produced, which causes expansion and internal stress in the concrete. The gel will damage the concrete if the following damage takes place: 1) there is a sufficient supply of reactive silica in the aggregate. 2) The concentration of OH^- ions in the concrete's solution increases. 3) Water can be obtained from an outside source. Alkali-silica reactivity seems to have been a problem that was resolved by: 1) applying non-reactive aggregate. 2) Using cement that contains less than 0.6 percent by mass of sodium oxide (Na_2O) equivalent low-alkali cement. 3) The maximum cement content is 500 kg/m^3. 4) Using silica fume, slag, and other substitutes to partially replace cement. 5) Using the salts with ASR dominance. 6) Avoiding any contact between concrete and a moisture source. The products of the alkali silica reaction fling the aggregates, increase calcium, and form the chemical formula C-S-H (Katayama T., 2010; Thaulow etal., 1996; Leemann, A et al., 2013). Li, Q et al. (2014), Hou, et al. (2013), Hou, et al. (2004), Hou, et al. (2005), and Hou, et al. ASR crystallization's subsequent steps were established through carefully monitored mortar mixture studies. It dissolves and reacts with calcium hydroxide (CaOH)

to generate calcium-silicate-hydrate (C-S-H) when OH^- ions attack silica, and this process continues until the nearby CH is consumed locally. The C-S-H at this stage is silica-rich and extremely limited. A hydrous ASR gel has a tendency to develop at this stage. This result supports Taylor's thesis that the chemical formula of ASR is mostly that of a pozzolanic reaction (Taylor, 1997). The phases of the reaction were confirmed by Li et al. (2014), who showed that the decrease of CH and the C-S-H reaction at 80 °C were necessary, that is the temperature that the widely accepted Standard ASTM test C1260 indicates. This reaction sequence provides a starting point for the microstructural variations discussed below. ASR happens when hydroxides in cementations materials react with high-reactivity silica in concrete. Alkali-silica gel can expand due to a reaction mechanism when the surrounding Portland cement's surrounding humidity is absorbed. The expansion may produce cracks in concrete. Most countries impose a limit on the typical amount of hydroxides (such Na_2O) in cementations materials to control or prevent ASR in concrete. However, it was later shown that the necessary ratio of 0.6 percent equivalent alkalis was insufficient to prevent damage to the ASR. If concrete buildings' alkaline cement rates have only been as low as (0.45-0.50) percent equivalent Na_2O. Stark, D. (1995). Aggregates that are reactive and that, when combined with sodium hydroxide, produce alkali silica gel as a consequence of the interaction between silicate and the alkali metal (NaOH). They consequently absorb water from their surroundings, stressing the concrete as a result. The existing alkaline content limitation of 0.6 allows for the control of the alkali aggregating reactivity. When applied to concrete pozzolanic materials, a different approach of controlling the alkali aggregate reaction yields stronger strength and less overall porosity. Rougher aggregate surfaces have higher strengths and smaller total porosities that come into touch with the cement paste than do rounded particles, which results in weaker concrete.

2. Materials and methods

2.1 Materials

The materials used in this study are aggregates, Ordinary Portland cement (OPC) and sand. Five samples of aggregates are examined in this study by XRD analyses and XRF analyses, which are mainly composed of calcite ($CaCO_3$), dolomite ($CaMg(CO_3)_2$) and quartz (SiO_2). Three limestone aggregate samples are supplied from El- Alameen area and the two dolomitic stone aggregate samples are derived from Attaqa area, Egypt. The cement is ordinary Portland cement with a grade of 42.5. (Suez Cement Company). Sand is quarried and obtained from Cairo's open quarries and El-Wahat El-Baharaya Road. The chemical compositions of the cement and aggregates were tested as shown in *Tables 1* and *2*. *Fig. 1* gives the chemical and mineralogical compositions of limestone aggregate samples (L) and the chemical and mineralogical of dolomitic stone aggregate samples (D) are derived from Attaqa area are given in *Fig. 2*. *Table 4* displays the physio-mechanical properties of limestone and dolostone aggregates.

Oxide content	Cement
L.O.I	2.92
MgO	1.45
SiO_2	20.47
Al_2O_3	4.48
SO_3	2.80
K_2O	0.29
CaO	60.88
Fe_2O_3	5.49
Na_2O	0.33

Table 1 Chemical compositions of cement (wt. %)
1. táblázat Cement kémiai összetétele (m %)

Oxide content	Samples				
	E2	E3	E4	D1	D2
Al_2O_3	1.39	1.39	1.34	3.03	4.45
CaO	48.35	53.60	53.30	36.50	46.78
Fe_2O_3	1.18	0.93	0.87	0.62	1.13
MgO	1.47	0.92	1.71	13.90	6.02
L.O.I	29.79	33.20	33.20	43.60	39.60
SiO_2	16.5	8.79	8.41	3.03	4.45

Table 2 Chemical compositions of aggregates (wt. %)
2. táblázat Adalékanyagok kémiai összetétele (m %)

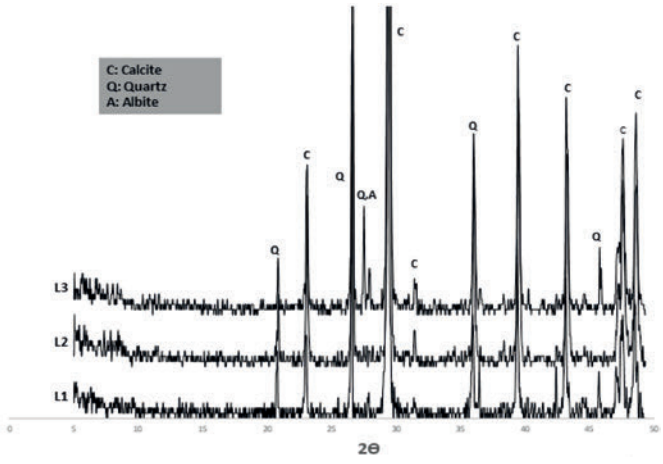

Fig. 1 The XRD pattern of limestone aggregate samples
1. ábra Mészkő adalékanyag XRD mintája

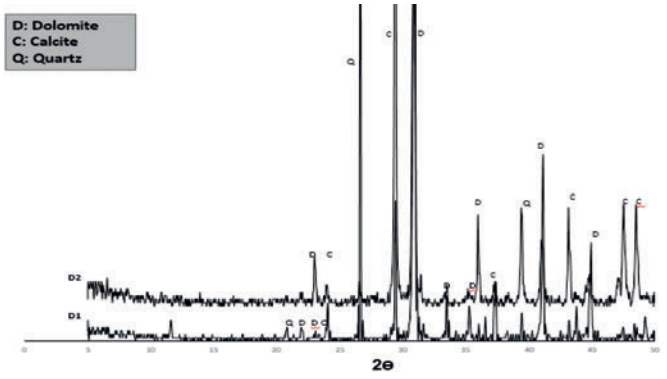

Fig. 2 The XRD pattern of dolomitic aggregate samples
2. ábra Dolomit adalékanyag XRD mintája

Physical parameters	L2	L3	L4	D1	D2
Water absorption (W_a)%	3	3.4	2.1	2.4	3.7
Specific gravity (G_{od})	2.8	2.9	2.6	2.7	3
Aggregate impact value (AIV)%	35	37	20	31	39
Flakiness index (I_F)%	41	41.5	20	24	43
Elongation index (I_E)%	29	32	23	23	32
Los Angeles abrasion value (LAV)%	42	42	25	26	43

Table 3 Physico mechanical properties of limestone and dolostone
3. táblázat Mészkő és dolomit fizikai-mechanikai tulajdonságai

W_a, G_{od}, AIV, I_F, I_E, and LAV have all been physical properties to their own minimum, maximum, and mean values measured in *Table 3*, Limits of roads and concrete aggregates are defined by BS and ASTM specifications, and also related BS and ASTM standards. According to ASTM-127, the W_a content of aggregate used in cement concrete will be less than 2.5 percent. This means these limestones meet the water absorption requirements for cement concrete. Calcite crystals have a specific gravity of 2.60 to 2.78, while concrete blocks require a lower limit around 2.60. It signifies that the specific gravity results from these stones are in the limits of ASTM C127.The physical qualities of flakiness and elongation index are connected to the geometry of aggregate fragments. High values cause reduced strength and anisotropic properties if used as aggregates in roadway and cement construction. The I_F and I_E value of the limestones vary around (12.20–1930) and (10.10–28.91), respectively, and are constrained by (BS 882 and 812:105. 2.) AIV is an indicator method for testing the compaction resistivity of an aggregate to rapid stress (Smith, Collis 2001). The range of LAV for these limestones is 14.08–25.12%, less than 40% as specified by ASTM C-131, which implies that these rocks can be used as road aggregate.

2.2 Methods

2.2.1 Alkali Silica Reaction

The accelerated mortar bar test (AMBT) is a technique employed by Oberholster and Davies at the National Building Research Institute in South Africa (1986). The proportion of cement to aggregates is 1:2.25, while the proportion of water to cement is 0.47. Casting mortar bars with the specified aggregate (coarse or fine) that has been treated to a defined gradation was part of the test. The concrete specimens were poured into (25x25x285) mm^3 cubic steal moulds in two equal levels with compacting each layer. The mortars bars were taken from their moulds after 24hrs and immersed in water at room temperature, which was then heated to 80°C in a drier for the next 24 hours where the mortar bars be stored at this temperature. After extracting the samples from water, they have been measured for length before becoming immersed in a 1N NaOH solution for 56 days at 80°C. Regular length change measurements were done during the storage period. Although different agencies define different expansion limits, most standards use the total expansion at the end of the 56 days soaking period. ASTM for example, have defined the following expansion requirements:
ASTM C 1260 expansion criteria:
< 0.10% is considered innocuous
0.10 to 0.20% is considered potentially reactive
> 0.20% is considered reactive

2.2.2 Alkali Carbonate Reaction

The concrete prism test (ASTM C 1105) is widely regarded as a much more fast and reliable method of estimating aggregate performance characteristics. This test uses concrete with a cement content of 420 kg/m^3. The equivalent alkali concentration of the cement should be between 0.8 and 1.0%. The proportions of water and cement were 0.42 to 0.45. The concrete prisms have dimensions of (75x75x285) mm^3. Molds made of cubic steal that have been cured for 24 hours at 23 °C and then stored at 38 °C over water. When examining plain concrete, measurements of expansion were conducted at periodic times with no chemical admixtures. Aggregates that increased by more than 0.04 percent in a year were referred as reactive aggregates.

3. Results and discussion

3.1 Alkali Silica Reaction (ASR)

3.1.1 Limestone aggregate from El-Alameen area (L)

The limestone aggregates used in the concrete originated from the El-Alameen region (D). The composition and quantity of gel had an impact on the expanding forces carried on by its presence in concrete. It appears that time has an impact on the reaction products' creation. ASR gel is produced in greater volume during a longer exposure time, resulting in a broader expansion (Kawamura M. et al., 1998) and (E. Gavrilenko et al., 2007), while the gel's composition changes over time. The gel initially took in water but not Na^+ or K^+ ions. The gel became increasingly viscous and expanded over the initial alkali-rich gel as the reactions continued and the gel's Ca^{2+} concentration increased. (Kawamura M. et al., 1998) found that elevated temperatures significantly increased the overall amount of Ca^{2+} in the concrete gel. This was thought to be necessary in order to produce expanding gel. Also, they found no evidence that the alkali silica gel's Ca^{2+} content had an impact on the gel's development rate. Alkali-silica reaction gel's viscosity flow was decreased by increasing the alkali content inside the gel. Alkali gels' viscosity may not be high enough to produce enough expanding force to crack aggregate concrete as a result.

Mix notation / Curing time, days	Linear expansion,%		
	L1	L2	L3
3	0	0.035	0.074
7	0.002	0.041	0.085
10	0.014	0.068	0.092
14	0.027	0.098	0.167
16	0.046	0.151	0.247
28	0.058	0.223	0.381
56	0.064	0.354	0.496

Table 4 Linear expansion values of (L) mixes cured in 1N NaOH up to 56 days
4. táblázat 56 napig 1N NaOH oldatban tárolt (L) keverékek lineáris tágulás értékei

Table 4 shows that the samples were left in the solution for longer than ASTM C 1260 specifies, and *Fig. 3* shows the data as a function of curing time up to 56 days. Since L1 did not exceed the allowed limits and generated improved results after 56 days, it was determined that L1 is the sample that is most resistant to high temperatures and soaking in sodium hydroxide.

L2 and L3 samples that started out performing poorly improved considerably and visibly as time passed on throughout the next 14 days. The generation of a huge volume of silica gel over an extended period of time and a correspondingly significant increase in length made Sample L3 the most extended sample.

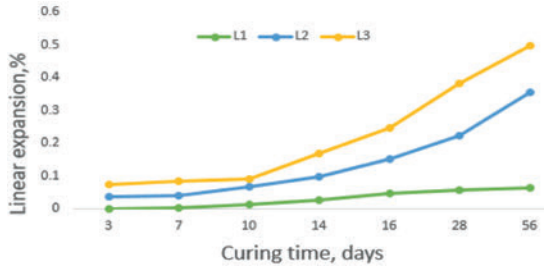

Fig. 3 Linear expansion values of (L) mixes cured in 1N NaOH up to 56 days
3. ábra 56 napig 1N NaOH oldatban tárolt (L) keverékek lineáris tágulás értékei

3.1.2 Dolomitic stone aggregate from Attaqa area (D)

These aggregates were collected from the Attaqa region (A). The ASR products generated have different contents, according to experiments on materials that were soaked in various dissolved salts. KOH produced more crystalline gel, whereas NaOH was more aggressive and produced more gel. The expansion increased until a particular amount of alkalis was reached, at which point it continued to shrink as the concentration of alkalis increased. The linear expansion values of the aggregates taken from Attaqa (A) are listed in *Table 5*, which is displayed as a function of the curing time in *Fig. 4*.

Mix notation Curing time, days5	Linear expansion,%	
	D1	D2
3	0.018	0.072
7	0.021	0.079
10	0.038	0.093
14	0.041	0.158
16	0.056	0.228
28	0.083	0.401
56	0.094	0.479

Table 5 Linear expansion values of (D) mixes cured in 1NaOH up to 56 days
5. táblázat 56 napig 1N NaOH oldatban tárolt (D) keverékek lineáris tágulás értékei

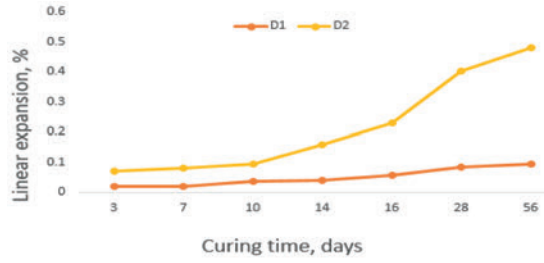

Fig. 4 Linear expansion values of (D) mixes cured in 1 NaOH up to 56 days
4. ábra 56 napig 1N NaOH oldatban tárolt (D) keverékek lineáris tágulás értékei

From this area, two samples were chosen, with Sample D1 being the best because it included a good aggregate and had a lower proportion of porosity than the other sample. This resulted in the creation of a significant amount of calcium silicate hydrate and a reduction in the rate of expansion at the age of 56 days. The limitations were actually strengthened by significantly expanding sample D3 due to the increased silica gel development, which has produced enough expanding force to crack concrete samples.

3.1.3 Products analysis (Scanning electron microscopy)

SEM micrographs of hardened specimens (D1) and (D2) after 56 days of curing are illustrated in *Fig. 5*. ASR gel appeared in cracks extending from reactive, fine-grained, dolomitic limestone coarse particles into the paste in plane-polarized transmitted light thin section electron microscopy. The ASR gel looked opaque in cross-polarized view, an unusual quality that typically sets it apart from other crystalline secondary deposits. The aggregates had a fine-grained calcite, clay, and quartz matrix with scattered, isolated dolomite rhombs as its main constituent. The dark gray, fine- grained dolomitic limestone coarse aggregates were the source of reactive silica for ASR. Si-rich phases in dolomitic limestone could exist locally in small regions and as extremely fine-grained, split silica particles intermingled with the rock matrix, in contrast to conventional alkali reactive siliceous rocks. Figure showed localized regions of cryptocrystalline quartz in the rock's matrix. As can be seen, silica occured in two different ways: first, as relatively large particles, and second, as much smaller particles mixed up with the matrix. The finer particles were potentially reactive silica minerals, but the coarser ones were detrital, non-reactive quartz.

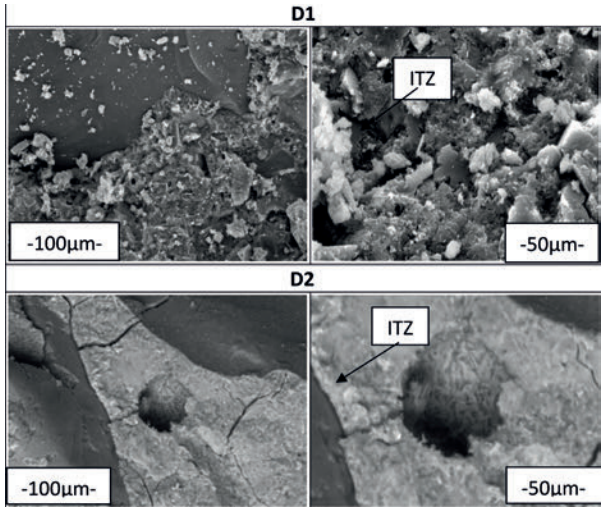

Fig. 5 SEM Photography of D1 and D2 immersed in 1N NaOH up to 56 days
5. ábra 56 napig 1N NaOH oldatban tárolt D1 és D2 SEM felvételei

3.2 Alkali Carbonate Reaction (ACR)

3.2.1 Limestone aggregate from El-Alameen area (L)

Limestone aggregates for concrete were collected from the El-Almeen region (L). Because of the interaction between the silica in limestones and the alkali components in OPC, an alkali silica gel has been created (Mustansar Naeem et al., 2019). The silica gel and calcite particles mixed together, which led to the aggregates' expansion. The gel that formed in the limestone also differed greatly. The sample seems to be larger and covers a significant portion of the surface. The linear expansion

values of concrete containing limestone are listed in *Table 6* and shown as a function of curing time in *Fig. 6*. In comparison to the other samples, Sample L1 started with a high expansion at a curing age of 7 days. Even so, the sample increased till the age of curing of 360 days, with convergence in the length of the sample expansion after reaching a similar expansion at the age of 180 days. Without a certainty, the sample L2 showed that it had expanded gradually up to the age of 360 days. Although the later sample performed significantly better at age 7 days, the expansion was higher than that of sample L1. Despite being a reactive aggregate, sample L3 exhibited the same behavior as the other samples. The expansion of L3 became really clear at the age of 360 days of curing.

Mix notation / Curing time, days	Linear expansion,%		
	L1	L2	L3
7	0.009	0.001	0.02
28	0.004	0.002	0.013
56	0.001	0.002	0.01
90	0.005	0.004	0.01
180	0.007	0.013	0.014
270	0.025	0.026	0.017
360	0.038	0.069	0.12

Table 6 Linear expansion values of (L) mixes cured over water up to 360 days
6. táblázat 360 napig víz alatt tárolt (L) keverékek lineáris tágulás értékei

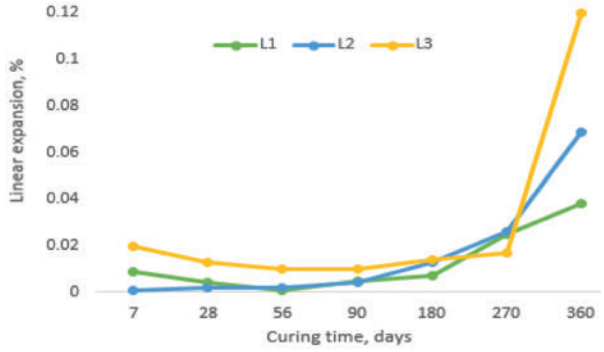

Fig. 6 Linear expansion values of (L) mixes cured over water up to 360 days
6. ábra 360 napig víz alatt tárolt (L) keverékek lineáris tágulás értékei

3.2.2 Dolomitic stone aggregate from Attaqa area (D)

Dolomite aggregate for concrete was extracted from the Attaqa region (A). When the silica in the dolomite concrete mix reacted with the alkali component in Portland cement, an alkali-silica gel was created. As the gel expanded and absorbed water, the calcite particles were compressed together. Once the gel had stretched the calcite crystals together, they had become clearly visible (M. Ahmed et al., 2018). As a result, the concrete and aggregate particles both increased. The gel that formed in the aggregates was quite different. The sample seemed to be bigger and covered a substantial portion of the surface. *Table 7* showed the linear expansion values of concrete containing dolomite aggregate, which are graphed as a function of curing time in *Fig. 7*. Sample D1 expanded more over the duration of 7 days to 56 days before decreasing at 90 days of curing and then expanding once more over the next 360 days till it reached the critical zone. After the age reached 360 days, the sample D2 expansion's length didn't stop expanding, indicating that it was still active. The sample's porosity increased as a result of its expansion, increasing water absorption and lowering the sample's mechanical characteristics.

Mix notation / Curing time, days	Linear expansion,%	
	D1	D2
3	0.018	0.072
7	0.021	0.079
10	0.038	0.093
14	0.041	0.158
16	0.056	0.228
28	0.083	0.401
56	0.094	0.479

Table 7 Linear expansion values of (D) mixes cured over water up to 360 days
7. táblázat 360 napig víz alatt tárolt (D) keverékek lineáris tágulás értékei

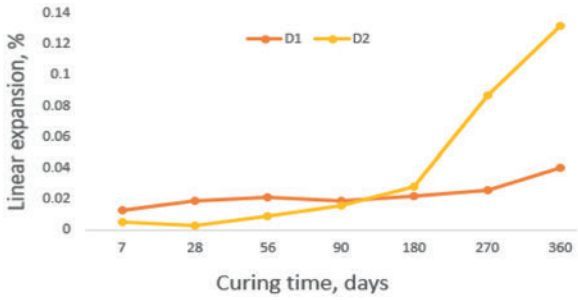

Fig. 7 Linear expansion values of (D) mixes cured over water up to 360 days
7. ábra 360 napig víz alatt tárolt (D) keverékek lineáris tágulás értékei

3.2.3 Products analysis (Scanning electron microscopy)

Polarizing microscopy revealed that ACR produced a micrographic texture within the reaction ring that was made up of brucite and calcite spots.

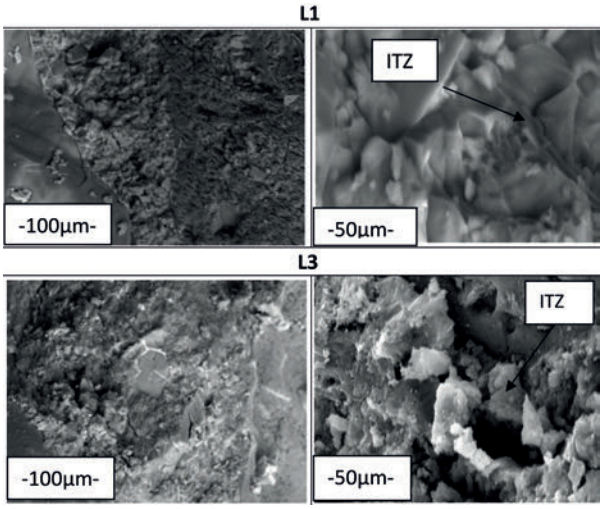

Fig. 8 SEM Photography of L1 and L3 cured over water up to 360 day
8. ábra 360 napig víz alatt tárolt L1 és L3 SEM felvételei

As seen in *Fig. 8*, SEM micrographs of hardened specimens (L1) and (L3) after 360 days of curing are plotted, aggregates with limestone-rich patches and cracks after reaction was chosen for observation using SEM and element materials mapping analysis in order to further explore the reason of expansion stress generated by alkali-carbonate reaction and

showed a large number of rod-shaped crystals next to the calcite. Calcite and brucite were the byproducts of the reaction between dolomite and alkali in aggregate. Because some of the dolomite had not completely reacted during the dedolomitization process, it is important to note that unreacted dolomite is still present in aggregate particles. Calcite ($CaCO_3$) was generated by ACR when the region was primarily made up of Ca, C, and O components. Moreover, when the region is primarily made up of Mg and O components, ACR will generate brucite ($Mg(OH)_2$). Expansion strain caused by the accumulation and development of brucite crystals, and the aggregate then went through an alkali-carbonate reaction to create expansion.

4. Conclusion

The goal of this study was that comparing between the concrete prism test (alkali carbonate reaction) over a 360-day period and the accelerated mortar bar test (alkali silica reaction) at 56 days. Five aggregate samples have been collected from the El-Alameen and Ataqaa areas. They were composed primarily of dolostone with some limestone. In comparison to the other samples, which were taken from the El Alameen region, Sample L1 demonstrated the least linear expansion of the accelerated mortar bar test (alkali silica reaction) at 56 days of curing and the least linear expansion of the concrete prism test (alkali carbonate reaction) at 360 days of curing. In every test, including the concrete prism test (alkali carbonate reaction) and the mortar bar test (alkali silica reaction), Sample D1 performed better than the other samples from the Ataqqa area. Mortar and concrete composed of limestone have an effect on the resistance of sodium hydroxide and reduce the production of silica gel than that composed of dolostone. The accelerated mortar bar test AMBT was time-efficient and comparable to the alkali carbonate reaction (ACR), which was shown to be more indicative of particular issues. The alkali carbonate reaction ACR succeeded in its objective, as shown by the accelerated mortar bar test AMBT. As was indicated before, the ages of 270 and 360 days in the concrete prism corresponded to the ages of 16, 28, and 56 days in AMBT. Because AMBT is utilized in the Egyptian Code for Laboratory Tests manual and is valid in all situations, it is assumed based on these earlier findings that AMBT fits and matches ACR.

References

[1] Ahmad M., Ansari M.K., Rajesh Singh, Sharma L.K., Singh T.N., Sandra Pires," Assessment of Potential Alkali Aggregate Reactivity for Siliceous and Carbonate Aggregates: A Case Study", JOURNAL GEOLOGICAL SOCIETY OF INDIA Vol.91, pp.467-474 (2018).

[2] ASTM Standard C1260, "Standard Test Method for Potential Alkali Reactivity of Aggregates" (Mortar-Bar Method), ASTM International, West Conshohocken, PA, 2014, https://doi.org/10.1520/C1260, (2014).

[3] ASTM C1105, "Standard Test Method for Length Change of Concrete Due to Alkali-Carbonate Rock Reaction", American Standard of Testing Materials ASTM-C, pp. 1-4, (2004).

[4] ASTM Standards, "Standard test method for the resistance to degradation of small-size coarse aggregates by abrasion and impact in the Los Angeles Machine", C127–04, v. 04.02, USA, (2006b).

[5] BS EN 12350-6,"Testing Fresh Concrete: Density", British Standard (2009).

[6] British Standard Institute "Methods for determination of Flakiness Index", BS 812.105.1, London, (1985).

[7] British Standard Institute "Methods for determination of elongation index", BS 812.105.2, London, (1990a).

[8] BS EN 12390-3, "Testing Hardened Concrete: Compressive Strength of testing Specimens", British Standard (2001).

[9] BS EN12390-7, "Testing Hardened Concrete: Density", British Standard (2009).

[10] Fecteau, P., Fournier, B., Choquette, M., and Duchesne, J., "Contribution of the understanding of the so-called alkali- carbonate reaction". 14th International Conference on Alkali Aggregate Reaction, Austin, Texas, USA, (2012).

[11] Gavrilenko E., Garcia del Amo D., Calvo Pérez B., Garcia Garcia E.," Comparison of ASR-gels in concretes against accelerated mortar bar test samples", Magazine of Concrete Research, 59 483-494, (2007).

[12] Hadley, D.W., "Alkali reactivity of Dolomitic Carbonate rocks. In Symposium on Alkali Carbonate Rock Reaction". Highway Res. Record No.45, 1-19 (244P), (1964).

[13] Hou, X.; Shin, J.-H.; Struble, L.J.; Kirkpatrick, R.J. "Chemical and Microstructural Changes Associated with Alkali-silica Reaction in Mortar" In Proceedings of the 35th International Conference on Cement Microscopy, Chicago, IL, USA, May (2013).

[14] Hou, X.; Struble, L.J.; Kirkpatrick, R.J. "Formation of ASR gel and the roles of C-S-H and portlandite". Cement and Concrete Research, 34, 1683–1696, (2004).

[15] Hou, X.; Struble, L.J.; Kirkpatrick, R.J.; Monteiro, P.J.M. "Structural investigations of alkali silicate gels". J. Am. Ceram. Soc., 88, 943–949, (2005).

[16] Katayama T., "The so-called alkali- carbonate reaction (ACR) - its mineralogical and geochemical details, with special reference to ASR". Cement and Concrete Research, 40, 643-675, (2010).

[17] Kawamura M., Arano N., Terashima T.," Composition of ASR gels and expansion of mortars," in: M. Cohen, S. Mindess, J. Skalny (Eds.) Materials Science of Concrete: Special Volume – The Sidney Diamond Symposium, Westerville, OH, pp. 261-276, (1998).

[18] Leemann, A.; Merz, C. "An attempt to validate the ultra-accelerated microbar and the concrete performance test with the degree of AAR-induced damage observed in concrete structures". Cement and Concrete Research, 49, 29–37, (2013).

[19] Mustansar Naeem, Tehseen Zafar, M. Touseef Bilal and Abiola Oyebamiji "Physical characterization and alkali carbonate reactivity (ACR) potential of the rocks from Bauhti Pind and Bajar area Hassan Abdal, Pakistan", (2019).

[20] Ozol, M. A.," Alkali carbonate rock reaction", in: P. Klieger, J.F. Lamond (Eds of Tests and Properties of Concrete and Concrete Making Mat.), Significance erials., 'Pennsylvania, pp. 372-387, (1994).

[21] Qiang Li, R. James Kirkpatrick, Leslie J. Struble "Alkali Silica Reaction in Mortar at Room Temperature". In Proceedings of ACI Special Proceedings in CD on Novel Characterization Techniques and Advanced Cementitious Materials: Tribute to James J. Beaudoin, Washington, DC, USA, 26–30, (2014).

[22] Smith, M. R. and Collis, L. (Eds). Aggregates: sand, gravel and crushed rock aggregates for construction purposes (3rd edition), Geological Society. London: Engineering Geology Special Publication No. 17, Revised by P.G. Fookes, J. Lay, I. Sims, M. R.Smith and G. West, 339 p ,(2001).

[23] Stark, D.: "Alkali-Silica Reaction and its Effects on Concrete". USCOLD 2nd international Conference on Alkali-Silica Reaction, Chattanooga, TN, (1995).

[24] Swenson, E.G., and, Gillott, J.E., "Alkali carbonate rock reaction". Highway Research, Record 45, 21-40, (1964).

[25] Tang, M., Liu, Z. & Han, S. "Mechanism of alkali–carbonate reaction". In: Grattan-Bellew, P.E. (ed.), Proceedings of the 7th International Congress on Alkali–Aggregate Reactions in Concrete. Ottawa, Canada, Noyes Publications, Park Ridge, NJ, 275–279, (1987).

[26] Taylor, H.F.W. Cement Chemistry, 2nd ed.; Thomas Telford: London, UK; pp. 361–365, (1997).

[27] Thaulow, N.; Jakobsen, U.H.; Clark, B. "Composition of alkali silica gel and ettringite in concrete railroad ties: SEM-EDX and X-ray diffraction analyses". Cement and Concrete Research 26, 309–318, (1996).

Ref.:
Mohamed, Reham Abu-Elwafa – **Zeedan**, Sayeada Rawwash: *The silica-alkaline reaction of aggregates is more realistic than the alkaline-carbonate reaction of aggregates*
Építőanyag – Journal of Silicate Based and Composite Materials, Vol. 76, No. 3 (2024), 113–118 p.
https://doi.org/10.14382/epitoanyag-jsbcm.2024.13

The analysis of composite piezo-magnetic beams into dynamic nonlocal nonlinear case

Ridha A. AHMED
an assistant professor in the Department of Computer Engineering of Mustansiriyah University, Baghdad, Iraq

Wael N. ABDULLAH
Research Scholar in the Department of Architectural Engineering, Mustansiriyah University, Baghdad, Iraq

Nadhim M. FALEH
Professor in the Department of Mechanical Engineering of Mustansiriyah University, Baghdad, Iraq

Ridha A. AHMED ▪ Department of Computer Engineering of Mustansiriyah University, Iraq ▪ ridhalwan@uomustansiriyah.edu.iq
Wael N. ABDULLAH ▪ Department of Architectural Engineering, Mustansiriyah University, Iraq ▪ wael.najm65@gmail.com
Nadhim M. FALEH ▪ Department of Mechanical Engineering of Mustansiriyah University, Iraq ▪ ridhalwan@uomustansiriyah.edu.iq

Érkezett: 2024. 10. 26. ▪ Received: 26. 10. 2024. ▪ https://doi.org/10.14382/epitoanyag-jsbcm.2024.14

Abstract
This paper investigates the nonlinear dynamical behaviour of piezo-magnetic beams using the formulation by a refined higher-order beam that incorporates nonlocal effects and the piezoelectric phase. The increase in the piezoelectric phase can enhance the vibrational behaviour of bright beams under magnetic fields and harmonic excitation. We have derived the nonlinear governing equations for a nonlocal intelligent beam based on the refined beam model, and a numerical method has been introduced to calculate the nonlinear vibrational curves. Our study shows that variations in the volume fraction of the piezoelectric material significantly impact the vibrational behavior of the intelligent nanobeam when exposed to electrical and magnetic fields. Additionally, the nonlinear free and forced vibrational behaviour of the intelligent nanobeam is influenced by the magnitudes of induced electrical voltages, magnetic potential, the stiffness of the elastic substrate, and shear deformation.
Keywords: composite, dynamic behaviour, forced vibration, vibration; piezoelectric, nonlocal
Kulcsszavak: kompozit, dinamikus viselkedés, kényszerrezgés, szabad vibráció; piezoelektromos erősítés, nem lokális elmélet

1. Introduction

Recent advancements in engineering materials have highlighted the benefits of smart or intelligent materials [1]. The incorporation of these innovative materials into various multifunctional structures has led to significant changes across different engineering fields. Among these materials, magneto-electro-elastic (MEE) materials stand out because they exhibit a unique triple energy change between elastic, electrical, and magnetic arenas [2-4]. As a result, they are promising candidates for sophisticated applications such as vibration control, sensors, energy harvesting, and actuators. Recently, researchers have focused on synthesising MEE structures with composite materials to enhance their structural functions. For example, the properties of multi-phase MEE materials might be worked by varying the composition and proportion of each phase [5,6]. Recognising the significance of intelligent structures made from MEE materials with different compositions in industrial contexts, many scholars have dedicated their research to evaluating mechanical responses in various operational environments [7, 8].

At the nanoscale, size effects have a significant impact on both physical and mechanical properties. This phenomenon has prompted researchers to investigate the mechanical response of nanostructures. The fundamental limitation of classical continuum mechanics is its inadequacy in modeling small-scale structures, which has led to the development of higher-order continuum theories that easily incorporate size dependency [9-14]. Eringen's nonlocal elasticity theory [15] has proven useful in addressing size effects. Due to the challenges associated with experimentally testing nanoscale structures, many articles have been published to optimize the use of this theory in assessing size-dependent structural responses [16-19]. These studies indicate that, with a higher nonlocal parameter value, nonlocal elastic models are effective in yielding a stiffness-softening effect.

Building on Eringen's nonlocal elasticity theory, some researchers have analysed MEE or piezo-magnetic nanostructures. For example, Ke and Wang [20] studied the linear vibrational properties of intelligent nanoscale beams using nonlocal theory. Additionally, Jandaghian and Rahmani [21] investigated the linear vibrational characteristics of intelligent nanoscale beams on elastic foundations. Ebrahimi and Barati [22] also examined the vibrational properties of a functionally graded intelligent nanoscale beam using nonlocal theory. In light of these findings, this article aims to develop a multi-phase MEE nanobeam resting on a nonlinear elastic substrate for dynamic analysis within the framework of nonlocal elasticity theory. An approximate solution is then provided based on Galerkin's technique. A parametric study is conducted to study the effect of nonlocality, various piezoelectric volumes, electromagnetic fields, and elastic substrate coefficients on the structural performance of these nanoscale systems. The results of this research have the potential to significantly impact the design and optimisation of innovative structures under dynamic loads, offering promising prospects for future research and development in this field.

At the nano range, the significant effect of size is noticed on both mechanical and physical properties. This case has interested a few authors in distracting their focus from assessing the mechanical response of the nanostructures. The main limitation of classical continuum mechanics is its disorganisation in modelling small-

size structures, which paved the way for the founding of higher-order continuum theories which join the size dependence of structure with ease [10-14]. Eringen's nonlocal elasticity theory [15] proved to be handy in employing the side effects. Because experimenting with nano-size structures is still hard, numerous articles have been available to best utilise this theory in evaluating size-dependent structural responses [16-19]. The primary result of these authors indicates that the higher value of the nonlocal parameter and nonlocal elastic models are efficient and sufficient only to yield a stiffness-softening effect. Joining Eringen's nonlocal elasticity theory, few authors tried to analyse the MEE or piezo-magnetic nanostructures. With the usage of nonlocal theory, a study on linear vibrational properties of intelligent nano-size beams has been represented by Ke and Wang [20]. Moreover, Jandaghian and Rahmani [21] represented linear vibrational investigation of intelligent nano-size beams based on elastic foundations. In another research, Ebrahimi and Barati examined the vibrational properties of a functionally graded intelligent nano-scale beam using nonlocal theory [17].

This article aims to develop a multi-phase magnetoelectric (MEE) nanobeam that rests on a nonlinear elastic substrate, focusing on dynamical analysis within the framework of nonlocal elasticity theory. We propose that the MEE composite consists of two phases, each containing piezoelectric and magnetic components. To investigate the nanoscale effects, we employ Eringen's elasticity theory.

The authors in this study derive the equilibrium equations of the nanobeam with properties of MEE by using Hamilton's method and von Kármán geometric nonlinearity. An approximate solution is then obtained using Galerkin's technique. Furthermore, a comprehensive parametric study is conducted to examine how nonlocality, various piezoelectric volume percentages, electromagnetic field effects, and elastic substrate coefficients influence the structural performance of these nanoscale systems. The findings of this paper have the potential to significantly impact the design and optimisation of innovative structures under dynamic loads, paving the way for future research and development in this promising field.

2. Two-phase composite

Fig. 1 illustrates a nanoscale beam made of a magneto-electro-elastic composite consisting of two phases. The material properties of this multi-phase magneto-electro-elastic (MEE) composite depend on the ratio and volume of the piezoelectric phase (Vf). This item focuses on a nanobeam constructed from a composite of $BaTiO_3$ and $CoFe_2O_4$. In this context, $BaTiO_3$ serves as the piezoelectric component, while $CoFe_2O_4$ acts as the piezomagnetic component.

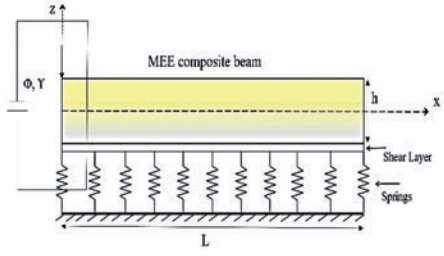

Fig. 1 A composite nanobeam rested on an elastic substrate
1. ábra Rugalmas anyagon nyugvó kompozit nanogerenda

3. Formulation due to refined beam theory

Different beam and plate theories are available in the literature [23-37]. This section will present the procedure for deriving the governing equations for a piezo-magnetic nanobeam within the framework of both nonlocal and classical beam theories. To achieve this, the displacement field of a nanoscale beam, based on axial (u) and transverse (w) displacements at the mid-axis, can be expressed as follows (Fourn et al. 2018):

$$u_1(x,z,t) = u(x,t) - z\frac{\partial w_b}{\partial x} - (z)\frac{\partial w_s}{\partial x} \tag{1}$$

$$u_2(x,z,t) = w(x,t) = w_b(x) + w_s(x) \tag{2}$$

Based on *Equations 1* and *2*, the authors applied mathematical treatments to derive the following equations:

Next, integrating *Equation 3* yields:

$$\frac{\partial u}{\partial x} = -\frac{1}{2}\left(\frac{\partial w}{\partial x}\right)^2 - \frac{A_{31}^e}{A_{11}}\phi - \frac{A_{31}^m}{A_{11}}\gamma + \frac{B_{11}}{A_{11}}\frac{\partial^2 w_b}{\partial x^2} + \frac{B_{11}^s}{A_{11}}\frac{\partial^2 w_s}{\partial x^2} + \frac{N_x^E}{A_{11}} + \frac{N_x^H}{A_{11}} + \frac{C_1}{A_{11}} \tag{3}$$

So, Satisfying edge settings; u(0)=0, u(L)=0, one can derive:

$$u = -\frac{1}{2}\int_0^x \left(\frac{\partial w}{\partial x}\right)^2 dx - \frac{A_{31}^e}{A_{11}}\int_0^x \phi dx - \frac{A_{31}^m}{A_{11}}\int_0^x \gamma dx + \frac{B_{11}}{A_{11}}\frac{\partial w_b}{\partial x} + \frac{B_{11}^s}{A_{11}}\frac{\partial w_s}{\partial x} + \frac{N_x^E}{A_{11}}\int_0^x dx + \frac{N_x^H}{A_{11}}\int_0^x dx + \frac{C_1}{A_{11}}x + C_2 \tag{4}$$

$$C_2 = -\left(\frac{B_{11}}{A_{11}}\frac{\partial w_b}{\partial x} + \frac{B_{11}^s}{A_{11}}\frac{\partial w_s}{\partial x}\right)_{x=0}$$

$$C_1 = \frac{A_{11}}{2L}\int_0^L \left(\frac{\partial w}{\partial x}\right)^2 dx + \frac{A_{31}^e}{L}\int_0^L \phi dx + \frac{A_{31}^m}{L}\int_0^L \gamma dx - \left(\frac{B_{11}}{L}\frac{\partial w_b}{\partial x} + \frac{B_{11}^s}{L}\frac{\partial w_s}{\partial x}\right)_{x=L} - (N_x^E + N_x^H) \tag{5}$$

As the next step, finded constant must be situated in *Equation 50*.

4. Solution method

In this study, the governing equations of motion for free/forced vibrations of simply-supported MEE nano-size beams have been solved by employing Galerkin's approach. The displacement functions are provided as a creation of non-unknown coefficients and identified trigonometric functions to promise the conditions of boundary at x=0 and x=L as [26]:

$$w_b = \sum_{p=1}^{\infty} W_{bp}(t)X_p(x) \tag{6}$$

$$w_s = \sum_{p=1}^{\infty} W_{sp}(t)X_p(x) \tag{7}$$

$$\phi = \sum_{p=1}^{\infty} \Phi_p(t)X_p(x) \tag{8}$$

$$\gamma = \sum_{p=1}^{\infty} \Upsilon_p(t)X_p(x) \tag{9}$$

where (W_{bp}, W_{sp}, Φ_p, γ_p) display the field largest values and the function $X_p = \sin(p\pi x / L)$ displays the shape function of the simply supported beam ($w = \frac{\partial^2 w}{\partial x^2} = \gamma = \phi = 0$). Placing *Equations 6–9* in governing equations yields below equations:

$$K_{1,1}^S W_{bp} + K_{2,1}^S W_{sp} + G_1 W_p^3 + Q_1 W_p^2 + M_1 \ddot{W}_p + K_1^E \Phi_p + K_1^H \Upsilon_p = F\cos(\omega t)$$
$$K_{1,2}^S W_{bp} + K_{2,2}^S W_{sp} + G_2 W_p^3 + Q_2 W_p^2 + M_2 \ddot{W}_p + K_2^E \Phi_p + K_2^H \Upsilon_p = F\cos(\omega t)$$
$$K_{1,3}^S W_{bp} + K_{2,3}^S W_{sp} + G_3 W_p^2 + K_3^E \Phi_p + K_3^H \Upsilon_p = 0$$
$$K_{1,4}^S W_{bp} + K_{2,4}^S W_{sp} + G_4 W_p^2 + K_4^E \Phi_p + K_4^H \Upsilon_p = 0 \quad (10)$$

By using KS as components of the stiffness matrix, Gi as stiffness of nonlinear . The overhead equations are concurrently resolved in order to get nonlinear vibration frequencies. Then the approximate solution has the below definition:

$$W_p(t) = \tilde{W}\ \cos(\omega t) \quad (11)$$

Also, dimensionless quantities are selected as:

$$K_L = \mathrm{k}_L \frac{\mathrm{L}^4}{D_{11}},\ K_p = \mathrm{k}_p \frac{\mathrm{L}^2}{D_{11}},\ K_{NL} = \mathrm{k}_{NL} \frac{\mathrm{L}^4}{A_{11}}$$
$$\tilde{\omega} = \omega L^2 \sqrt{\frac{\rho A}{\tilde{c}_{11} I}}, \mu = \frac{ea}{L}, \tilde{F} = F \frac{L^2}{A_{11} h} \quad (12)$$

5. Numerical results and discussions

In this section, we have presented several graphical examples and discussed the results obtained to validate the free vibrational properties of multi-phase MEE nano-sized beams. The results, based on the assumption of a geometrically perfect nanobeam, have been provided. The length of the nano-scale beam is set at L = 10 nm. To ensure the reliability of our approach, we have compared our findings with the work of Li et al. [16] regarding the non-linear vibration frequencies of imperfect nanobeams based on various maximum vibration amplitudes. This comparison serves to affirm the robustness of our model, as our results align with those reported by Li et al. [16].

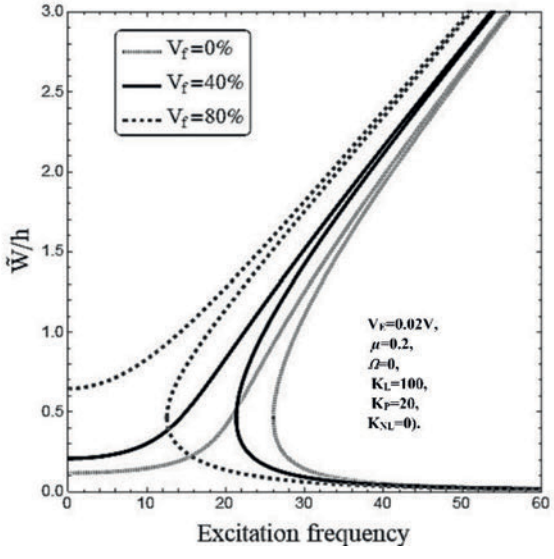

Fig. 2 Impact and voltage on vibration frequency curves of the nanobeam
2. ábra A nanogerenda rezgési frekvenciájára gyakorolt hatás és feszültség

The influence of piezoelectric volume on forced vibrational curves of the nanobeam is shown in *Fig. 2*, $\tilde{F}$=0.01. The volume of piezoelectric ingredients has been selected to be V_f=0%, 40% and 80%. From the figure, it may be understood that enhancing the volume of piezoelectric ingredients yields lower shift frequencies. This is associated with the decrement in the elastic stiffness of nano-scale beams by increasing the piezoelectric portion. Afterwards, the elastic modulus of composites decreases by increasing the piezoelectric ingredient. Also, as the magnitude of electric voltage is lower, the curves are closer to each other. Accordingly, an MEE nano-scale beam with higher percentages of piezoelectric ingredients is more susceptible to induced electrical fields.

Fig. 3 provides a comparison among non-linear frequencies based upon classical and improved (refined) shear deformation beam types of MEE nano-sized beams. The presented graph has been illustrated according to the hypothesis that the aspect ratio is L/h=10. This figure highlights that non-linear vibrational curves tend to have higher frequencies when the magnitudes of non-dimension deflection grow. Such observation is associated with stiffening influences of non-linear geometrical factors. Moreover, one may understand that improved beam theory grants more minor non-linear vibrational frequencies than classical theory because of the impact of the insertion of shear deformation. Hence, the improved theory is more reliable for a thick intelligent piezoelectric-magnetic beam.

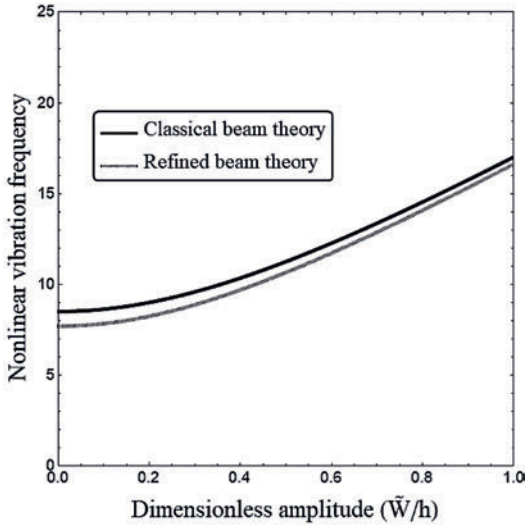

Fig. 3 a comparison among non-linear frequencies of MEE nano-sized beam
3. ábra Az MEE nano-méretű gerenda nemlineáris frekvenciáinak összehasonlítása

Fig. 4 illustrates the effect of tiny scales on the non-linear vibrational frequency of a two-phase magnetoelectric (MEE) nanoscale beam in relation to normalised vibrational amplitudes. It is evident that as the parameter of dimensionless nonlocal (μ) increases, the normalised frequency decreases. This indicates that classical elastic theory, which does not account for small-size effects, tends to provide higher approximations for normalised vibrational frequency. In contrast, nonlocal continuum mechanics offers greater precision and reliability, resulting in more accurate outcomes.

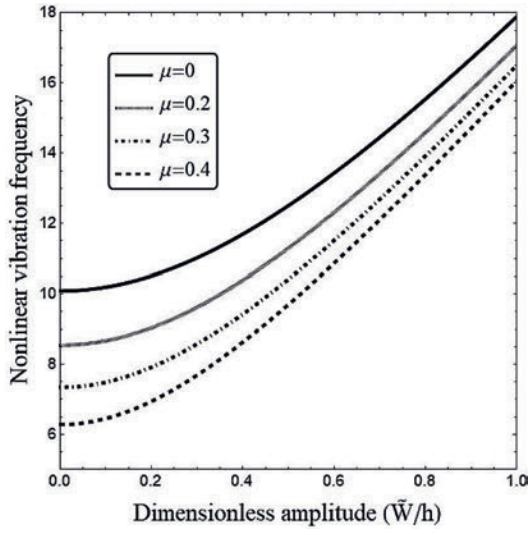

Fig. 4 The effect of small scales on the non-linear vibrational frequency
4. ábra A kis méretek hatása a nemlineáris rezgési frekvenciára

Fig. 5 displays changes in non-linear vibration frequency versus normalised amplitude under various electric voltages (VE) and magnetic field intensities (Ω). Notably, the non-linear shift frequency decreases as the applied electric field transitions from negative to positive voltages. Similarly, an increase in magnetic field intensity from negative to positive results in a rise in non-linear vibration frequency. This phenomenon can be attributed to the exceptional capacity of MEE materials to absorb and maintain magnetism. As the intensity of the magnetic field increases, this ability becomes more pronounced, facilitating the conversion of magnetic potential into mechanical force. Consequently, as the magnetic field exerts tensile forces on the nanobeam, the non-linear vibration frequency increases.

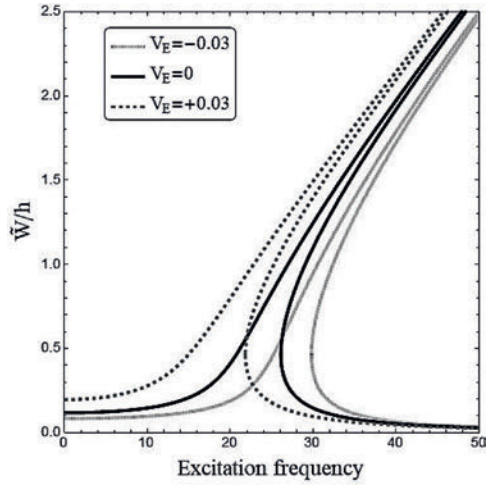

Fig. 5 The changes in non-linear vibration frequency
5. ábra A nemlineáris rezgási frekvencia változásai

6. Conclusion

This research investigates the fascinating dynamics of nonlocal, nonlinear free and forced vibrations in two-phase magneto electro elastic (MEE) nanobeams, presenting an insightful analytical perspective. These nanobeams are modeled to rest on an elastic foundation characterized by three key parameters: linear, shear, and nonlinear.

Notably, our findings reveal that as the dimensionless nonlocal parameter increases – indicating the significance of nonlocal effects – the normalized frequency, which is independent of system size, correspondingly decreases. This clearly illustrates that the classical elastic model, which neglects small-scale effects, produces inflated estimates of the non-dimensional vibrational frequency.

Moreover, the study highlights an intriguing trend: the nonlinear foundation parameter significantly influences vibration frequency curves, particularly as vibration amplitude rises. It is also crucial to note that the interaction of the magnetic field with the vibration characteristics of MEE nanobeams is contingent upon the piezoelectric volume. Yet, as the piezoelectric volume increases, the rate of frequency enhancement in response to magnetic field intensity diminishes. This underscores the complexity and interdependence of these parameters, reinforcing the importance of considering them in future research.

Acknowledgement

The authors sincerely rise the invaluable support from Mustansiriyah University (www.uomustansiriyah.edu.iq) in Iraq, which has been instrumental in the achievement of this work.

References

[1] Sahu, S. A., Singhal, A. and Chaudhary, S. (2018), "Surface wave propagation in functionally graded piezoelectric material: an analytical solution," Journal of Intelligent Material Systems and Structures, 29(3), 423-437. https://doi.org/10.1177%2F1045389X17708047.

[2] Singhal, A., Sahu, S. A. and Chaudhary, S. (2018), "Liouville-Green approximation: An analytical approach to study the elastic waves vibrations in composite structure of piezo material. Composite Structures, 184, 714-727. https://doi.org/10.1016/j.compstruct.2017.10.031.

[3] Pan, E. and Han, F. (2005), "Exact solution for functionally graded and layered magneto-electro-elastic plates," International Journal of Engineering Science, 43(3-4), 321-339. https://doi.org/10.1016/j.ijengsci.2004.09.006.

[4] Li, L. and Hu, Y. (2016), "Critical flow velocity of fluid-conveying magneto-electro-elastic pipe resting on an elastic foundation. International Journal of Mechanical Sciences, 119, 273-282. https://doi.org/10.1016/j.ijmecsci.2016.10.030.

[5] Mirjavadi, S. S., Forsat, M., Nikookar, M., Barati, M. R and Hamouda, A. M. S. (2019), "Nonlinear forced vibrations of sandwich smart nanobeams with two-phase piezo-magnetic face sheets," The European Physical Journal Plus, 134(10), 508. https://doi.org/10.1140/epjp/i2019-12806-8.

[6] Ahmed, R. A., Fenjan, R. M. and Faleh, N. M. (2019), "Analyzing post-buckling behavior of continuously graded FG nanobeams with geometrical imperfections," Geomechanics and Engineering, 17(2), 175-180. https://doi.org/10.12989/gae.2019.17.2.175.

[7] Kumaravel, A., Ganesan, N. and Sethuraman, R. (2007), "Buckling and vibration analysis of layered and multiphase magneto-electro-elastic beam under thermal environment. Multidiscipline Modeling in Materials and Structures, 3(4), 461-476. https://doi.org/10.1163/157361107782106401.

[8] Annigeri, A. R., Ganesan, N. and Swarnamani, S. (2007), "Free vibration behaviour of multiphase and layered magneto-electro-elastic beam," Journal of Sound and Vibration, 299(1-2), 44-63. https://doi.org/10.1016/j.jsv.2006.06.044.

[9] Boutaleb, S., Benrahou, K. H., Bakora, A., Algarni, A., Bousahla, A. A., Tounsi, A. and Mahmoud, S. R. (2019), "Dynamic analysis of nanosize FG

rectangular plates based on simple nonlocal quasi 3D HSDT," Advances in nano research, 7(3), 191. https://doi.org/10.12989/anr.2019.7.3.191.

[10] Tlidji, Y., Zidour, M., Draiche, K., Safa, A., Bourada, M., Tounsi, A. and Mahmoud, S. R. (2019), "Vibration analysis of different material distributions of functionally graded microbeam. Structural Engineering and Mechanics, 69(6), 637-649. https://doi.org/10.12989/sem.2019.69.6.637.

[11] Semmah, A., Heireche, H., Bousahla, A. A. and Tounsi, A. (2019), "Thermal buckling analysis of SWBNNT on Winkler foundation by non local FSDT. Advances in nano research, 7(2), 89. https://doi.org/10.12989/anr.2019.7.2.089.

[12] She, G. L., Ren, Y. R., Yuan, F. G. and Xiao, W. S. (2018), "On vibrations of porous nanotubes. International Journal of Engineering Science, 125, 23-35. https://doi.org/10.1016/j.ijengsci.2017.12.009.

[13] Saffari, S., Hashemian, M. and Toghraie, D. (2017), "Dynamic stability of functionally graded nanobeam based on nonlocal Timoshenko theory considering surface effects," Physica B: Condensed Matter, 520, 97-105. https://doi.org/10.1016/j.physb.2017.06.029.

[14] Soltani, K., Bessaim, A., Houari, M. S. A., Kaci, A., Benguediab, M., Tounsi, A. and Alhodaly, M. S. (2019), "A novel hyperbolic shear deformation theory for the mechanical buckling analysis of advanced composite plates resting on elastic foundations. Steel and Composite structures, 30(1), 13-29. https://doi.org/10.12989/scs.2019.30.1.013.

[15] Eringen, A. C. (1972), "Linear theory of nonlocal elasticity and dispersion of plane waves. International Journal of Engineering Science, 10(5), 425-435. https://doi.org/10.1016/0020-7225(72)90050-X.

[16] Li, L., Tang, H. and Hu, Y. (2018), "Size-dependent nonlinear vibration of beam-type porous materials with an initial geometrical curvature. Composite Structures, 184, 1177-1188. https://doi.org/10.1016/j.compstruct.2017.10.052.

[17] Al-Maliki, A. F., Faleh, N. M. and Alasadi, A. A. (2019), "Finite element formulation and vibration of nonlocal refined metal foam beams with symmetric and non-symmetric porosities," Structural Monitoring and Maintenance, 6(2), 147-159. https:// doi.org/10.12989/smm.2019.6.2.147.

[18] Uzun, B. and Civalek, Ö. (2019), "Free vibration analysis Silicon nanowires surrounded by elastic matrix by nonlocal finite element method. Advances in nano research, 7(2), 99. https://doi.org/10.12989/anr.2019.7.2.099.

[19] Wu, C. P., Chen, Y. H., Hong, Z. L. and Lin, C. H. (2018), "Nonlinear vibration analysis of an embedded multi-walled carbon nanotube. Advances in nano research, 6(2), 163. https://doi.org/10.12989/anr.2018.6.2.163.

[20] Ke, L. L. and Wang, Y. S. (2014), "Free vibration of size-dependent magneto-electro-elastic nanobeams based on the nonlocal theory. Physica E: Low-Dimensional Systems and Nanostructures, 63, 52-61. https://doi.org/10.1016/j.physe.2014.05.002.

[21] Jandaghian, A. A. and Rahmani, O. (2016), "Free vibration analysis of magneto-electro-thermo-elastic nanobeams resting on a Pasternak foundation. Smart Materials and Structures, 25(3), 035023. https://doi.org/10.1088/0964-1726/25/3/035023.

[22] Ebrahimi, F. and Barati, M. R. (2017), "Surface effects on the vibration behavior of flexoelectric nanobeams based on nonlocal elasticity theory. The European Physical Journal Plus, 132(1), 19. https://doi.org/10.1140/epjp/i2017-11320-5.

[23] Hassan, W.N.F.W., Ismail, M.A., Lee, H.S., Meddah, M.S., Singh, J.K., Hussin, M.W., & Ismail, M. (2020). Mixture optimization of high-strength blended concrete using central composite design. Construction and Building Materials, 243, 118251.

[24] Abdelaziz, H. H., Meziane, M. A. A., Bousahla, A. A., Tounsi, A., Mahmoud, S. R. and Alwabli, A. S. (2017), "An efficient hyperbolic shear deformation theory for bending, buckling and free vibration of FGM sandwich plates with various boundary conditions," Steel and Composite Structures, 25(6), 693-704. https://doi.org/10.12989/scs.2017.25.6.693.

[25] Atmane, H.A., Tounsi, A., Bernard, F. and Mahmoud, S.R. (2015), "A computational shear displacement model for vibrational analysis of functionally graded beams with porosities", Steel and Composite Structures, 19(2), 369-384. https://doi.org/10.12989/scs.2015.19.2.369.

[26] Barati, M. R. (2017), "Nonlocal-strain gradient forced vibration analysis of metal foam nanoplates with uniform and graded porosities," Advances in nano research, 5(4), 393. https://doi.org/10.12989/anr.2017.5.4.393.

[27] Bellifa, H., Bakora, A., Tounsi, A., Bousahla, A. A. and Mahmoud, S. R. (2017), "An efficient and simple four variable refined plate theory for buckling analysis of functionally graded plates. Steel and Composite Structures, 25(3), 257-270. https://doi.org/10.12989/scs.2017.25.3.257.

[28] Besseghier, A., Heireche, H., Bousahla, A. A., Tounsi, A. and Benzair, A. (2015), "Nonlinear vibration properties of a zigzag single-walled carbon nanotube embedded in a polymer matrix," Advances in nano research, 3(1), 029. https://doi.org/10.12989/anr.2015.3.1.029.

[29] Boukhlif, Z., Bouremana, M., Bourada, F., Bousahla, A. A., Bourada, M., Tounsi, A. and Al-Osta, M. A. (2019), "A simple quasi-3D HSDT for the dynamics analysis of FG thick plate on elastic foundation," Steel and Composite Structures, 31(5), 503-516. https://doi.org/10.12989/scs.2019.31.5.503.

[30] Bounouara, F., Benrahou, K. H., Belkorissat, I. and Tounsi, A. (2016), "A nonlocal zeroth-order shear deformation theory for free vibration of functionally graded nanoscale plates resting on elastic foundation. Steel and Composite Structures, 20(2), 227-249. https://doi.org/10.12989/scs.2016.20.2.227.

[31] Chaabane, L. A., Bourada, F., Sekkal, M., Zerouati, S., Zaoui, F. Z., Tounsi, A. and Tounsi, A. (2019), "Analytical study of bending and free vibration responses of functionally graded beams resting on elastic foundation. Structural Engineering and Mechanics, 71(2), 185-196. https://doi.org/10.12989/sem.2019.71.2.185.

[32] Fenjan, R. M., Ahmed, R. A., Alasadi, A. A. and Faleh, N. M. (2019), "Nonlocal strain gradient thermal vibration analysis of double-coupled metal foam plate system with uniform and non-uniform porosities. Coupled Syst Mech, 8(3), 247-257. https://doi.org/10.12989/csm.2019.8.3.247.

[33] Karami, B., Janghorban, M. and Tounsi, A. (2017), "Effects of triaxial magnetic field on the anisotropic nanoplates. Steel and composite structures, 25(3), 361-374. https://doi.org/10.12989/scs.2017.25.3.361.

[34] Mahmoudi, A., Benyoucef, S., Tounsi, A., Benachour, A., Adda Bedia, E. A. and Mahmoud, S. R. (2019), "A refined quasi-3D shear deformation theory for thermo-mechanical behavior of functionally graded sandwich plates on elastic foundations," Journal of Sandwich Structures & Materials, 21(6), 1906-1929. https://doi.org/10.1177%2F1099636217727577.

[35] Medani, M., Benahmed, A., Zidour, M., Heireche, H., Tounsi, A., Bousahla, A. A. and Mahmoud, S. R. (2019), "Static and dynamic behavior of (FG-CNT) reinforced porous sandwich plate using energy principle," Steel and Composite Structures, 32(5), 595-610. https://doi.org/10.12989/scs.2019.32.5.595.

[36] She, G. L., Yan, K. M., Zhang, Y. L., Liu, H. B. and Ren, Y. R. (2018), "Wave propagation of functionally graded porous nanobeams based on non-local strain gradient theory. The European Physical Journal Plus, 133(9), 368. https://doi.org/10.1140/epjp/i2018-12196-5.

[37] Zarga, D., Tounsi, A., Bousahla, A. A., Bourada, F. and Mahmoud, S. R. (2019), "Thermomechanical bending study for functionally graded sandwich plates using a simple quasi-3D shear deformation theory," Steel and Composite Structures, 32(3), 389-410. https://doi.org/10.12989/scs.2019.32.3.389.

[38] Fourn, H., Atmane, H. A., Bourada, M., Bousahla, A. A., Tounsi, A. and Mahmoud, S. R. (2018), "A novel four variable refined plate theory for wave propagation in functionally graded material plates. Steel and Composite Structures, 27(1), 109-122. https://doi.org/10.12989/scs.2018.27.1.109.

Ref.:
Ahmed, Ridha A. – **Abdullah**, Wael N. – **Faleh**, Nadhim M.: *The analysis of composite piezo-magnetic beams into dynamic nonlocal nonlinear case*
Építőanyag – Journal of Silicate Based and Composite Materials, Vol. 76, No. 3 (2024), 119–123 p.
https://doi.org/10.14382/epitoanyag-jsbcm.2024.14

GUIDELINE FOR AUTHORS

The manuscript must contain the followings: title; author's name, workplace, e-mail address; abstract, keywords; main text; acknowledgement (optional)**; references; figures, photos with notes; tables with notes; short biography** (information on the scientific works of the authors).

The full manuscript should not be more than 6 pages including figures, photos and tables. Settings of the word document are: 3 cm margin up and down, 2,5 cm margin left and right. Paper size: A4. Letter size 10 pt, type: Times New Roman. Lines: simple, justified.

TITLE, AUTHOR

The title of the article should be short and objective.

Under the title the name of the author(s), workplace, e-mail address.

If the text originally was a presentation or poster at a conference, it should be marked.

ABSTRACT, KEYWORDS

The abstract is a short summary of the manuscript, about a half page size. The author should give keywords to the text, which are the most important elements of the article.

MAIN TEXT

Contains: materials and experimental procedure (or something similar), results and discussion (or something similar), conclusions.

REFERENCES

References are marked with numbers, e.g. [6], and a bibliography is made by the reference's order. References should be provided together with the DOI if available.

Examples:

Journals:

[6] Mohamed, K. R. – El-Rashidy, Z. M. – Salama, A. A.: In vitro properties of nano-hydroxyapatite/chitosan biocomposites. *Ceramics International.* 37(8), December 2011, pp. 3265–3271, http://doi.org/10.1016/j.ceramint.2011.05.121

Books:

[6] Mehta, P. K. – Monteiro, P. J. M.: Concrete. Microstructure, properties, and materials. *McGraw-Hill*, 2006, 659 p.

FIGURES, TABLES

All drawings, diagrams and photos are figures. The **text should contain references to all figures and tables**. This shows the place of the figure in the text. Please send all the figures in attached files, and not as a part of the text. **All figures and tables should have a title**.

Authors are asked to submit color figures by submission. Black and white figures are suggested to be avoided, however, acceptable.

The figures should be: tiff, jpg or eps files, 300 dpi at least, photos are 600 dpi at least.

BIOGRAPHY

Max. 500 character size professional biography of the author(s).

CHECKING

The editing board checks the articles and informs the authors about suggested modifications. Since the author is responsible for the content of the article, the author is not liable to accept them.

CONTACT

Please send the manuscript in electronic format to the following e-mail address: femgomze@uni-miskolc.hu and epitoanyag@szte.org.hu or by post: Scientific Society of the Silicate Industry, Budapest, Bécsi út 122–124., H-1034, HUNGARY

We kindly ask the authors to give their e-mail address and phone number on behalf of the quick conciliation.

Építőanyag – *Journal of Silicate Based and Composite Materials*, Quarterly peer-reviewed periodical of the Hungarian Scientific Society of the Silicate Industry, SZTE.
http://epitoanyag.org.hu